Enzyme-Mediated Proteolysis of Fibrous Biopolymers: Dissolution Front Movement in Fibrin or Collagen Under Conditions of Diffusive or Convective Transport

Sriram Anand, Jung-He Wu, and Scott L. Diamond*
Bioengineering Laboratory, Department of Chemical Engineering, The State University of New York, Buffalo, New York 14260

Received January 17, 1995/Accepted May 25, 1995

A numerical model based on the convective-diffusive transport of reacting and adsorbing proteolytic enzymes within erodible fibrous biopolymers was used to predict lysis fronts moving across biogels such as fibrin or collagen. The fiber structure and the transport properties of solutes in fibrin (or collagen) were related to the local extent of dissolution within the dissolving structure. An accounting for solubilization of adsorbed species into solution from the eroding fiber phase provided for complete conservation of mass in reacting systems containing over 10 species. At conditions of fibrinolysis typical of clinical situations, the model accurately predicted the dynamic rate of lysis front movement for plasmin, urokinase, and tissue plasminogen activator (tPA)-mediated lysis of fibrin gels measured in vitro. However, under conditions of extremely fast fibrinolysis using high enzyme concentrations, fibrinolytic fronts moved very rapidly (>0.1 mm/mm)—faster than predicted for diffusion-limited reactions—at nearly constant velocity for over 2 h, indicating non-Fickian behavior. This was due to proteolysis-mediated retraction of dissolving fibrin fibers that resulted in fiber convection and front-sharpening within 3 μm of the reaction front, as observed by digitally enhanced microscopy. In comparing the model to fibrinolysis measurements using human lys_{77}-plasmin, the average first order rate constant for non-crosslinked fibrin bond cleavage by fibrin-bound plasmin was calculated to be 5 s^{-1}, assuming that 10 cleavages per fibrin monomer were required to solubilize each monomer. The model accurately predicted lysis front movement using pressure-driven permeation of plasmin or urokinase into fibrin as well as literature data obtained under well-mixed conditions for tPA-mediated fibrinolysis. This numerical formulation provides predictive capability for optimization of proteolytic systems which include thrombolytic therapy, wound healing, controlled drug release, and tissue engineering applications. © 1995 John Wiley & Sons, Inc.

Key words: fibrin • collagen • proteolysis • plasminogen • diffusion.

INTRODUCTION

The transport phenomena of proteolytic enzymes that degrade fibrous protein structures are largely unexplored in spite of the importance of these processes during cell adhesion and cell migration in normal, pathologic, or artificial tissue structures. The immobilization of cultured cells in collagen matrices for bioreactor or biomedical applications is well established, yet the rates of proteolytic processes during matrix colonization are poorly understood. Additionally, tumor metastasis and cell migration during wound healing or tissue remodeling involve orchestrated expression of collagen, collagenases, plasminogen activators, and cellular receptors for the purpose of collagen and fibrin degradation and matrix remodeling. Both collagen and fibrin (or their chemically modified forms) are useful for the purposes of drug/cell delivery or programmed cell migration. Finally, the dissolution of blood clots by intravenous or intracoronary infusion of plasminogen activators such as streptokinase, urokinase (uPA), or tissue plasminogen activator (tPA) is a widely used clinical therapy for reperfusion of clot-blocked vessels. Thrombolytic therapy is a process characterized by the dispersive-convective penetration of proteolytic enzymes that bind the erodible fibrin fibers that compose a blood clot.[2,11,61]

Unique to the problem of protease transport—as opposed to the well-studied problem of protein diffusion in porous media[26,38,45]—is the dynamic binding of the enzyme to the solid protein structure with subsequent dissolution of the solid phase by the bound protease and solubilization of the enzyme back into the interstitial fluid. Also, in eroding systems, structural and biochemical properties such as porosity, pore radius, and binding sites are continually evolving.

The structural biology of fibrin and collagen is well established[12,16,64] and there are many similarities (Fig. 1). Both are comprised of monomeric proteins (fibrinogen and procollagen) that become activated by enzymatic cleavage and subsequently polymerize. The thrombin-activated fibrin monomers polymerize into extended protofibrils (two monomers thick) that aggregate laterally to form thick fibers. Peptidase activation of procollagen generates the tropocollagen monomer which polymerizes into microfibrils (five monomers thick) that aggregate again into fibrils which then aggregate into even thicker collagen fibers.

* To whom all correspondence should be addressed.

© 1995 John Wiley & Sons, Inc.
CCC 0006-3592/95/020089-19

Steric accessibility of sites on the surface and within the fiber may be quite relevant, especially for collagen fibers. Structural and transport properties of these fiber systems are given in Table I. While fibrin is the single polymeric network of fresh blood clots, interstitium in the human body contains collagen fibrils and fibers as well as elastin, glycoaminoglycans, and structural glycoproteins (and sometimes fibrin). The specific permeability and solute diffusivity in interstitial collagen is strongly influenced by these additional constituents.[30]

Fibrinolysis is a multicomponent and multiphase reaction network (Fig. 2). uPA can activate plasminogen to plasmin in a homogeneous fluid phase reaction,[31] whereas tPA can bind fibrin and activate fibrin-bound plasminogen (23) in a heterogeneous reaction. Plasminogen activator inhibitor type 1 (PAI-1) and α_2-antiplasmin inhibit plasminogen activators (uPA and tPA) and plasmin, respectively. Both inhibitors are ineffective when their targets are bound to fibrin.[22,32,58] As fibrin is cleaved by plasmin, new binding sites for plasminogen, plasmin, and tPA are revealed with the generation of carboxyterminal lysines[53] which may be subsequently removed by carboxypeptidases in plasma. Numerous biochemical complexities include the plasmin-mediated conversion of: prourokinase to urokinase; single-chain tPA to two-chain tPA; glu_1-plasminogen to lys_{77}-plasminogen; and glu_1-plasmin to lys_{77}-plasmin.[8,9,25,51] Each of these species has its own unique fibrin affinity and catalytic properties. The rates of key processes are given in Table II.

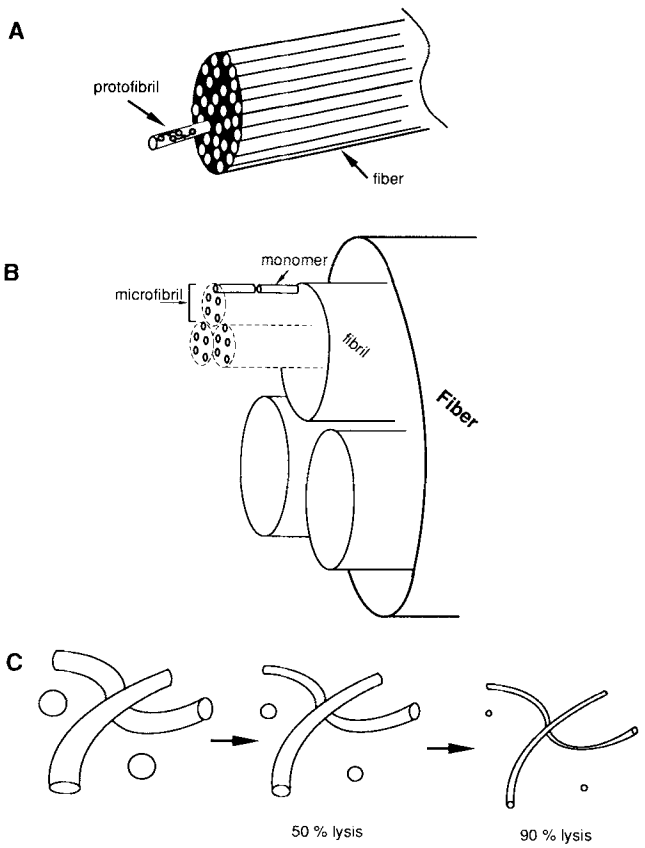

Figure 1. Each fibrin fiber is a bundle of many protofibrils (A). The protofibril is a staggered arrangement of fibrin monomers. Protofibrils present throughout the fiber bundle have specific binding sites which bind soluble species. For collagen fibers, the monomer extends to form microfibrils that aggregate to form fibrils which aggregate again to form fibers (B). Schematic model depicting the dissolving of fibers by protease degradation (C). As the fibers are lysed, the diameter of the fiber decreases while the length of the fiber remains constant that is, lysis proceeds radially inward.

Collagen degradation involves the action of collagenases and gelatinases as well as the participation of various inhibitors. Procollagenase is converted by a variety of enzymatic pathways to active collagenase[21] that can bind rapidly to fibrillar collagen. It is known that only the outer layer of fibers in the collagen matrix (constituting about 10% of the total collagen in the gel) are capable of binding collagenase.[55] Additional binding or cleavage sites within the fiber become sterically accessible upon significant degradation of the collagen matrix.[55] The rate of collagen cleavage by the protease (e.g., human fibroblast collagenase [HFC] or interstitial collagenase) depends on the type of collagen, the type of collagenase and the physical properties of the collagen fiber. The kinetics of collagenolysis have been studied[46,55] and the k_{cat} has been found to be 0.007 s^{-1} for HFC on human interstitial collagen. α_2-Macroglobulin is known to be the primary inhibitor of HFC, and has an affinity about 150 times higher than the affinity of collagenase for collagen.[14] Human skin fibroblasts also produce a collagenase inhibitor which is less active than α_2-macroglobulin.[56] Collagen can be extensively crosslinked and is less susceptible to lysis.[21] Rates of key steps are given in Table III.

Macromolecules diffuse in pores of molecular dimension at rates significantly slower than in bulk solution.[39] The diffusion of a macromolecule is retarded significantly when the ratio of the hydrodynamic radius of the macromolecule to the effective pore radius is in excess of 0.1 to 0.3.[4,5,40] The excluded fluid volume near the porous surface depends on the actual structure of the fibrous network;[15,36] however, the porosity in fibrin or interstitial collagen is typically in the range 0.7 to 0.99 and the effect of excluded volume on diffusion is likely small. In general, the effective diffusion coefficient is a function of the length scale ratio mentioned above, but it depends also on the viscosity of the solvent (water, glycoaminoglycan, and so forth) which fills the pore space. The fibrin gels considered in the present study have effective pore diameters larger than 100 nm and the enzymes have a nominal size on the order of 5 nm, thus hindrance effects are small. In collagen, the hindrance/viscosity effects due to glycoaminoglycan can be significant, whereas the collagen fiber network typically produces substantially less hindrance.[30,45] In biopolymers, an important factor in solute mobility is the adsorption/desorption with the immobile fiber phase. Due to binding interaction with the fiber network, a protein moves significantly slower compared with bulk diffusion. The effect of adsorption on diffusion has been studied by Kaufman et al.[26] In some cases, the measurement of the apparent diffusion coefficient

Table I. Structural and transport properties of fibrin and collagen.

	Fibrin	Collagen
Monomer size (dry)	Fibrinogen (340 kDa) 45 nm × 2 nm	Procollagen (300 kDa) 280 nm × 1.5 nm
Radius of hydrated fibril (r_o)	3–5 nm protofibril (2 monomers/fibril)	2–2.5-nm microfibril (5 monomers/microfibril) 5–150 nm fibrils (10–1000 microfibrils/fibril)
Radius of hydrated fiber (R_f)	4–50 nm (fine gel at 0.3 *M* NaCl) 100–500 nm (coarse gel at 0.1 *M* NaCl)	*O* (1 μm) fiber (10–500 fibrils/fiber) *O* (10 μm) fiber bundle (10–100 fibers/fiber bundle)
Diameter of pore (D_{pore})	0.1 (fine) to 10 μ*M* (coarse)	*O* (μm) collagen *O* (nm) glycoaminoglycan
Density of subunit in hydrated fiber cross-section (p_o)	0.01116 fibrils/nm^2 (coarse) 0.008366 fibrils/nm^2 (fine)	0.05225–0.07742 microfibril/nm^2 fibril 10–200 fibrils/μm^2 fiber 0.26–0.36 monomer/nm^2 microfibril 0.25–0.36 monomer/nm^2 fibril 0.1–0.14 monomer/nm^2 fiber {at 100 fibrils/μm^2 of fiber with 70 nm diameter fibrils}
Fiber porosity	0.80 (coarse)	0.483–0.6512 (fibril) 0.813–0.912 (fiber)
Fiber density	210 mg/mL fiber (fine) 280 mg/mL fiber (coarse)	465–689 mg/mL fibril 178–249 mg/mL fiber
Overall porosity (ϵ)	>0.99 (plasma gel) 0.9–0.99 (platelet-retracted clots) 0.75–0.9 (compacted fibrin)	0.9–0.99 (reconstituted) 0.7–0.8 (subcutaneous/aorta) 0.5–0.7 (cartilage)
Specific permeability (k)	10^{-8} cm^2 (coarse) to 10^{-12} cm^2 (fine)	10^{-12} to 10^{-14} cm^2
Peclet number (Pe) = $v \cdot L/D_L$	0 to *O* (10^3)	0 to *O* (10^2)
$\Delta P/L$	~60 mmHg/cm clot (arterial) 0 to 10 mmHg/cm/clot (venous)	1 to 60 mmHg per ~0.1–0.3 cm (lymphatic drainage)

$$\epsilon \frac{\partial c_i}{\partial t} = (s_i - c_i)\frac{\partial \epsilon}{\partial t} - (1 - \epsilon)\frac{\partial N_i^T}{\partial t} + \nabla \cdot (\mathbf{D} \bullet \nabla (\epsilon c_i)) - \nabla \cdot (\epsilon c_i \mathbf{v}) + \epsilon \sum_l \sum_k \mathcal{R}_{lk}^i \qquad (1)$$

rate of change in free phase | gain due to solid volume change (solubilization) | net adsorption (desorption) to solid | diffusion and dispersion | permeation | homogeneous reaction

for a binding protein can be system dependent, if the protein has a binding interaction that is not at local equilibrium.

Heterogeneous reactions can cause a change in solid volume due to phase change. This class of reactions is commonly treated by a "shrinking core" model, whereas the "progressive conversion" model is used for reaction systems that have no change in solid shape.[18,29] Despite some similarities with these models, the fiber degradation problem cannot be completely described by the principles which guide the above systems. The fiber radius is less than 1 μm and the fibers are themselves highly porous. During lysis, it is likely that both surface erosion and inner fiber dissolution occur simultaneously. However, the relative extents are not known, and may depend on specific reaction conditions. Substantial changes in fiber structure occur during lysis (as will be discussed in the Results section). Also, during the course of lysis, the porosity of the biopolymer gel increases and consequently the permeability increases. Most importantly, the enzymes present in the solid phase are released into the free phase when the fiber is lysed and are available for subsequent rounds of binding and reaction. In the next section, we present a mathematical model describing dynamic binding, reaction, and proteolysis of a fibrous biopolymer in the presence of species which catalyze and inhibit the rates of reaction.

THEORY

For transport in eroding heterogeneous media, the instantaneous concentration of a diffusible species at some position in the fluid phase of the gel is described by Eq. (1).[1,17,57] See Nomenclature for definition of variables. The rate of change of the local species concentrations in the fluid phase depends on the net adsorption rate to the solid fiber phase, dispersion, convective permeation, homogeneous reaction in the free phase, and the effects due to change of volume of the solid phase as species are released during solubiliza-

Table II. Adsorption and catalytic rate constants of fibrinolysis (f = free, b = bound). See Diamond and Anand[11] for details.

	Kinetic constants	Reference
Reversible adsorption		
fbn + $plg^f \rightleftharpoons plg^b$	Glu-plasminogen:	35
	K_d = 38 μM	
	$k_f = 1.087 \times 10^{-4}\ \mu M^{-1}\ s^{-1}$	($q_{glu\text{-}plg}$ = 2.0 sites/monomer)
	$k_r = 4.131 \times 10^{-3}\ s^{-1}$	
	Lys-plasminogen:	
	K_d = 0.5 μM	
	$k_f = 1.087 \times 10^{-4}\ \mu M^{-1}\ s^{-1}$	
	$k_r = 5.435 \times 10^{-5}\ s^{-1}$	($q_{lys\text{-}plg}$ = 2.4 sites/monomer)
fbn + $plm^f \rightleftharpoons plg^b$	Glu-plm or lys-plasmin:	51
	K_d = 0.5 μM	
	$k_f = 0.5 \times 10^{-3}\ \mu M^{-1}\ s^{-1}$	(q_{plm} = 2.0 sites/monomer)
	$k_r = 5.435 \times 10^{-5}\ s^{-1}$	
fbn + $tPA^f \rightleftharpoons tPA^b$	K_d = 0.58 μM	24
	$k_f = 0.95833 \times 10^{-4}\ \mu M^{-1}\ s^{-1}$	
	$k_r = 6.658 \times 10^{-5}\ s^{-1}$	(q_{tPA} = 1.5 sites/monomer)
Reaction		
plg^b + $tPA^b \rightarrow plm^b$	Glu-plasminogen:	23
	$k_2 = 0.10\ s^{-1}$	Bowes melanoma tPA
	K_m = 0.16 μM	
	Lys-plasminogen:	
	$k_2 = 0.2\ s^{-1}$	
	K_m = 0.02 μM	
	Recombinant human tPA:	64
	$k_2 = 15.0\ s^{-1}$	
	K_m = 0.13 μM	
plg^f + uPA → plm^f	Glu-plasminogen:	33
	$k_2 = 3.6\ s^{-1}$	
	K_m = 78 μM	
	Lys-plasminogen:	
	$k_2 = 4.6\ s^{-1}$	
	K_m = 3.8 μM	
	Two-chain urokinase	9
	$k_2 = 1.0\ s^{-1}$	
	K_m = 50.0 μM	
fbn + $plm^b \rightarrow$ FDP	Glu or lys-plasmin:	34, 62
	k_{cat} = 5 to 25 sec^{-1}	
plm^f + α_2-AP → [pl − AP]	Glu or lys-plasmin:	
	$k'' = 10\ \mu M^{-1}\ s^{-1}$	59
tPA^f + PAI → [tPA − PAI]	$k'' = 29\ \mu M^{-1}\ s^{-1}$	32
uPA^f + PAI → [uPA − PAI]	$k'' = 20\ \mu M^{-1}\ s^{-1}$	32
plg^f + α_2-AP $\rightleftharpoons$ [plg − AP]	K_d = 4.0 μM	60
	$k_f = 1.087 \times 10^{-4}\ \mu M^{-1}\ s^{-1}$	
	$k_r = 4.348 \times 10^{-4}\ s^{-1}$	

tion of the solid phase and free phase species are diluted in the lost solid volume. In general, the rate of change of a bound phase concentration of the ith species depends on the rate of binding, dissociation, and heterogeneous reaction [Eqs. (2) and (3)] where the jth species may compete for the rth binding site (ξ_{rj} = 1 interaction; ξ_{rj} = 0 no interaction) as shown in Eq. (2).

$$\frac{\partial N_i^T}{\partial t} = k_{f,i}^r(c_i)\left(\theta_r - \sum_j \xi_{rj} s_j\right) - k_{r,i}^r(s_i) \qquad (2)$$

rate of transfer between the two phases — adsorption — desorption

$$\frac{\partial s_i}{\partial t} = \frac{\partial N_i^T}{\partial t} + \sum_l \sum_k {}^sR_{lk}^i \qquad (3)$$

rate of change in solid phase — rate of transfer — heterogeneous reaction

Here, R_{lk}^i refers to fluid phase reactions and ${}^sR_{lk}^i$ refers to solid phase reactions, and are functions given as $R(c_l,c_k)$ or ${}^sR(s_l,s_k)$ that affect the ith species. The type of reaction (e.g., zero, first, and second order and Michaelis–Menten) and the rate coefficients are set a priori in user-defined matrices. Eq. (1) can be written for a one-dimensional problem as:

Table III. Adsorption and catalytic rate constants of collagen degradation (f = free, b = bound).

	Kinetic constants	References
Reversible adsorption		
Collagenase^f + collagen $\rightleftharpoons$collagenase^b	$K_d = 0.95\ \mu M$ $k_f = 0.5 \times 10^{-3}\ \mu M^{-1}\ s^{-1}$ $k_r = 0.475 \times 10^{-3}\ s^{-1}$	55
Reaction		
Collagenase^b + collagen $\rightarrow$solubilized collagen	$k_{cat} = 0.007$–$0.01854\ s^{-1}$	46, 55
Collagenase^f + α_2-macroglobulin $\rightarrow$[collagenase – α_2-macroglobulin]	$k_{cat} = 0.48\ s^{-1}$ $K_i = 171\ nM$	14

$$\epsilon \frac{\partial c_i}{\partial t} = (s_i - c_i) \frac{\partial \epsilon}{\partial t} - (1 - \epsilon) \frac{\partial N_i^T}{\partial t} + \frac{\partial (D_L \epsilon)}{\partial x} \cdot \frac{\partial c_i}{\partial x} + D_L \epsilon \frac{\partial^2 c_i}{\partial x^2} + \frac{\partial (D_L c_i)}{\partial x} \frac{\partial \epsilon}{\partial x} + D_L c_i \frac{\partial^2 \epsilon}{\partial x^2} - \left[v_x \frac{\partial (\epsilon c_i)}{\partial x} + (\epsilon c_i) \frac{\partial v_x}{\partial x} \right] + \epsilon \sum_l \sum_k R_{lk}^i \qquad (4)$$

The convection terms in Eq. (4) reduce to $\bar{v} \cdot (\partial c_i / \partial x)$ for one-dimensional flow, where $\bar{v} = \epsilon v_x$. The superficial velocity for pressure-driven permeation through fibrin or collagen can be accurately described by Darcy's law[6,30] where $\bar{v} = k/\mu\ (\Delta P/L)$. In the present formulation, we do not consider the possibility that the solid phase can undergo deformation or translation. In the absence of a pressure drop, the convection term is zero. For well-mixed systems, such as dispersed fiber suspensions, the concentration gradients are zero. If the longitudinal dispersion is not a function of local porosity, since the gels are quite porous (no hindered diffusion) (37) and the change in local dispersion is very weakly coupled to changing structure for an initially highly porous system, D_L need not be included in the differential operators.

We have used the Danckwerts boundary condition for conservation of species flux across the inlet for the boundary condition in the transport simulations. For simulations under well-mixed conditions, the initial concentrations across the entire domain were uniform (spatial derivative equal to zero), and species fluxes across the boundaries were set to zero, resulting in an initial value problem.

In fibrous media, the Brownian diffusion may be hindered,[40] depending on the relative size of the solute and the pore diameter [Eq. (5)]. Also, dispersion will occur during pressure-driven permeation.[44] The quantitative prediction of dispersion of reacting/adsorbing solutes in time-dependent random fibrous media is not fully established, and the correlation formulated in Eq. (6) was used with α and β equal to one. The convective velocity can be predicted for a given pressure drop across the media, based on material properties to estimate the specific permeability[13,27] [Eq. (7)] or by available permeability data.[3,6,30] Correlations for the specific permeability, such as the Davies equation[11,13] or the Carman–Kozeny equation,[27,30] are based on the fiber radius (or fiber surface area) and the gel porosity. These correlations, however, are less accurate in the high porosity ranges ($\epsilon > 0.9$) encountered with fibrin or collagen gels. Alternatively, the superficial velocity may be a known constant and no estimate of the specific permeability is needed. The contribution of impermeable cells entrapped in either collagen or fibrin is not expected to contribute significantly to the permeability of the structure, even at fairly high cell densities.[30] While the glycoaminoglycan within collagen typically has a larger contribution to the overall specific permeability, collagen fibrils or fibers may also offer significant resistance to permeation, depending on the particular tissue.

$$\mathcal{D}_{i,\text{eff}} = \text{function}(D_i, D_{\text{fiber}}, \epsilon) \qquad (5)$$

$$D_L = \mathcal{D}_{i,\text{eff}} + \alpha D_{\text{pore}} \mathbf{v}^{\beta} \qquad (6)$$

$$k = \text{function}(D_{\text{fiber}}, \epsilon) \qquad (7)$$

In eroding structures, it is necessary to relate the proteolysis rate with evolving matrix properties (R_f, ϵ, k). By evaluation of the instantaneous rate of cutting $\{\mathcal{R}(x',t'), \mu M/s\}$ based on the solid phase volume at some location x' at some time t' [Eq. (8)], it is possible to calculate the historic amount of cutting $\{\xi(x',t'), \mu M$ of cuts made at x' and $t'\}$ [Eq. (9)]. In defining a solubilization factor, γ, that relates the number of equivalent monomers solubilized to the number of cleavages made, the amount of solubilization or lysis $\{L(x',t'), \mu M$ of protein lysed at x' and $t'\}$ from the solid phase can be defined as a function of the historic amount of cuts made by the protease at position x'. For fibrin, the solubilization factor has been estimated to be a constant with a value of 0.1. This corresponds to the estimate that for every 10 cleavages by plasmin, an equivalent of one subunit of fibrin is solubilized.[41] A similar factor appears appropriate for collagen. This approach does not account for any dependence of plasminogen activating activity or plasmin activity on the actual radius of the fiber which is known to exist with very thin fibrils.[19] It is possible that γ increases as a structure becomes highly de-

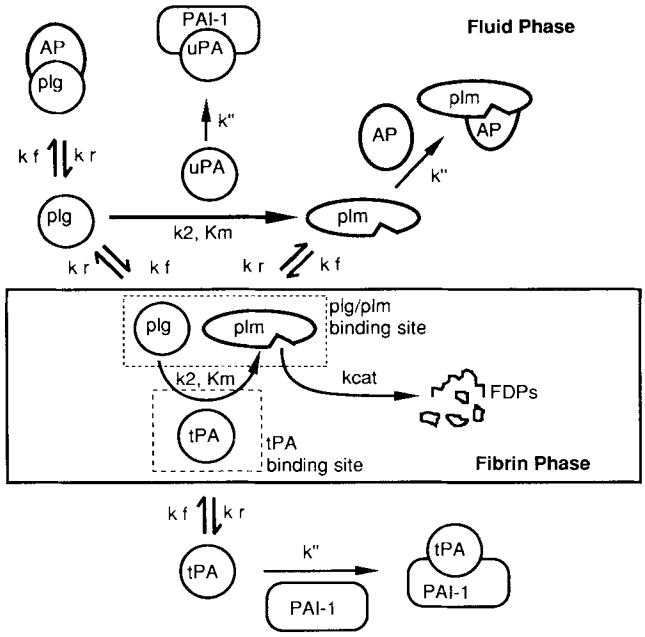

Figure 2. Summary of the fibrinolytic reaction pathway. Plasminogen (plg) is activated to plasmin (plm) in the solution phase by urokinase (uPA) while fibrin-bound plasminogen is activated by tissue plasminogen activator (tPA) in the fibrin phase. The free phase plasmin is inhibited by the antiplasmin, while the bound phase plasmin is protected from inhibition. The uPA and tPA are inhibited in the free phase by plasminogen activator inhibitor, type 1 (PAI-1). The association of plasmin with α_2-antiplasmin (AP) and the plasminogen activators with PAI-1 has been assumed to be irreversible. Soluble species can reversibly adsorb and desorb with fibrin. Plasminogen and plasmin compete for the same sites on the intact fibrin monomer whereas tPA binds a unique site. Each site can bind only one molecule at a time. All kinetic constants for reversible adsorption and irreversible enzymatic reaction are given in Table II.

graded, but this dependence has not been characterized experimentally.

$$\mathcal{R}(x',t') = k_{\text{cat}}\, s_i^{\text{protease}} \tag{8}$$

$$\xi(x',t') = \int_0^{t'} \mathcal{R}(x',t)dt \tag{9}$$

$$L(x',t') = \gamma \cdot \xi(x',t') \tag{10}$$

The bound protease concentration in the fiber and the solubilization rate are based on the solid fiber volume. Thus, the kinetic formulation lends itself to a progressive conversion model, and protease gradients in the fiber are not calculated. However, we have experimentally found using contrast-enhanced DIC microscopy that fibrin fibers appear to dissolve under certain conditions[61] with reduction of outer radius which indicates a shrinking core system. Thus, we have assumed that the fiber is solubilized at constant density. Reaction and solubilization throughout the fiber causes a loss of structural integrity that results in a collapse of the fiber at constant density and thus reduction of the fiber radius (Fig. 1C). This approach avoids the difficulty of calculating the dynamic spatial gradients for species within a micron-sized fiber that itself resides within a fibrin or collagen gel that has macroscopic dynamic spatial gradients.

To quantify the solid phase volume changes upon lysis, the total length of fibers initially in the gel must first be evaluated. Because fibers of collagen and fibrin have a relatively uniform initial radius R_{fo}, the total length of fibers is related to the fiber density (ρ_{fiber}), the gel density (ρ = g protein/vol$_T$) and the total volume, vol$_T$ (cm^3). The total length of fibers per volume of gel is given as:

$$L_T/\text{vol}_T = \rho \cdot \frac{10^{21}\ \text{nm}^3/\text{cm}^3}{\rho_{\text{fiber}}\,(\pi R_{fo}{}^2)} \text{ for } L_T \text{ and } R_{fo}\ [=]\ \text{nm} \tag{11}$$

If proteolysis proceeds from the outside of the fiber inward, the total length of fibers per unit volume of the gel, L_T/vol_T, is constant with time (Fig. 1C). To evaluate the binding sites within each fiber, it was necessary to know the number of protofibrils (fibrin) or microfibrils (collagen) within each fiber (Fig. 1A and B). The total number of protofibrils, N, contained in a fiber bundle of R_f can be calculated from the fiber density as follows:

$$\rho_{\text{fiber}} = \frac{\dfrac{MW}{N_{av}}\, N(\text{monomers per unit length})(L\text{-fibril})}{\pi R_f^2\ 10^{-21}\ \dfrac{\text{cm}^3}{\text{nm}^3}\ (L\text{-fiber})} \tag{12}$$

Because L-fibril is equal to L-fiber for fibrils oriented in the direction of the fiber, the number of protofibrils in a fibrin fiber is given as: $N = (0.035061)\ R_f^2$ for $R_f\ [=]$ nm using $\rho_{\text{fiber}} = 0.28$ g/mL.[7,11] The protofibril density $p_o = N/(\pi R_f^2)$ in the fiber is 0.01116 fibrils/nm^2 of fiber cross-sectional area for coarse fibrin. Similar values derived for collagen gel systems are given in Table I.

Knowing the amount of monomeric fibrin or collagen in a fiber than is lysed [Eq. (10)], we can directly calculate the local fiber radius, the volume of fibrin lysed off the fiber, and the local porosity in the gel at any instant in time by geometric argument. To maintain constant ρ_{fiber} or constant monomer concentration ($s_o = \rho_{\text{fiber}}/MW_{\text{monomer}}$), while the fiber radius R_f shrinks due to a local extent of lysis (L) requires:

$$R_f(x,t)^2 = R_{fo}^2\,(s_O - L(x,t))/s_O \tag{13}$$

For an initial fiber radius of R_{fo} and a total fiber density L_T/vol_T, the initial gel porosity is:

$$\begin{aligned}\epsilon_O &= 1 - \pi(R_{fo})^2\,(L_T/\text{vol}_T)10^{-21}\ \text{cm}^3/\text{nm}^3 \\ &= 1 - \rho_o/\rho_{\text{fiber}}\end{aligned} \tag{14}$$

The local instantaneous porosity $\epsilon(x,t)$ based on the local fiber radius $R_f(x,t)$, is calculated similarly. The percent lysis which is a common experimental measurement of solubilization is given at any position as:

$$\% \text{ Lysis}(x,t) = [1 - (R_f(x,t)/R_{fo})^2] \cdot 100 = L(x,t)/s_O \cdot 100 \quad (15)$$

The binding sites were defined by the following relation assuming that the total volume of the fiber was available (sterically accessible) for binding[11]:

$$m(R_f) = p_O \pi (R_f + r_O)^2 \quad (16)$$

If only a fixed number of "shells" of protofibrils or microfibrils are accessible, then the number of protofibrils which reside within $\kappa \cdot r_O$ of the outer radius, R_f, of the fiber can be expressed as:

$$m(R_f) = \int_0^{2\pi} \int_{R_f - \kappa r_O}^{R_f + r_O} p_O \, r \, dr \, d\theta = 4 \, p_O [2R_f r_O(1 + \kappa) + r_O^2(1 - \kappa^2)] \quad (17)$$

This is equivalent to n shells of protofibril which participate in fibrinolysis where $n = (\kappa + 1)/2$. The concentration of a given binding site (based on the solid phase volume), θ_i is directly related to the number of monomeric units available per unit fiber volume where q_i is the site number per monomer (Tables II and III).

$$\theta_i, \ \mu M \ i\text{th site} = q_i \cdot \{m(R_f)\} \cdot \frac{L_T}{\text{vol}_T} \cdot y \cdot \frac{1}{N_{av}} \frac{(10^6 \ \mu\text{mol/mol})}{(10^{-3} \ \text{L/cm}^3)} \quad (18)$$

where y = number of monomers per unit length of protofibril or microfibril. In some systems, q_i may be a function of percent lysis, because new binding sites are known to be generated in degraded fibrin.[50,53] We have kept q_i constant in the present work. The local specific permeability $k(x,t)$ can be calculated from $\epsilon(x,t)$ and $R_f(x,t)$ [Eq. (7)] using relations such as the Davies equation[11,13] or the Carman–Kozeny formulation.[27] At any given time, t', the overall specific permeability $\bar{k}$ can be evaluated as the inverse of the total resistivity by integrating the local resistivity $[k(x,t')]^{-1}$ over the length of the clot for a one-dimensional system.

NUMERICAL METHODS

The finite difference algorithm used to solve the system of equations is shown in Figure 3. The system of $2N + 1$ partial differential equations is coupled and nonlinear, where N is the number of participating species. Also, the transport and material properties (D_L, k, ϵ) change in time and space. To begin, the values are known for the free and bound concentrations, the fiber radius, porosity, and percent lysis at every node in the domain at the j time level. A two-step procedure was used to advance the solution from the j to the $j + 1$ time level via a differencing formulation at the $j + 1/2$ time level.[17,20,48] Therefore, initial guesses for the concentrations at the $j + 1/2$ level were made with a first order Taylor series expansion using the finite difference expression for the derivatives at the j time level.

At this point in the calculation, two different approaches were possible. The first approach was to use the estimated concentration of the bound protease at the $j + 1$ level (see third box of Fig. 3) to calculate solubilization at the $j + 1$ level, which was then integrated to obtain the amount of fiber lysed in an interval of time Δt. Knowing the amount of fiber lysed in Δt allowed calculation at the $j + 1$ level of the fiber radius and porosity, with subsequent determination of specific permeability and the permeation velocity. An improved material property guess at the $j + 1/2$ level for the porosity and fiber radius provided for a straightforward solution of c^{j+1}. The second approach would be to use directly the initial guess of the bound phase concentration obtained by Taylor series at the $j + 1/2$ level to calculate the solubilization rate and the relevant transport properties. This would yield the porosity, fiber radius, and velocity directly at the intermediate level and eliminate the averaging step. We have tried both these approaches—the first method was more robust and conserved mass of all species to a much greater level of tolerance. The first approach separated the calculation of the percent lysis and related properties from the calculation of the concentrations. Note that the second scheme would have required the calculation of the lysis to be embedded in the calculation of the bound phase concentration.

Upon calculation of the transport properties at the $j + 1/2$ and $j + 1$ level, the free phase concentrations at the $j + 1$ time level can be obtained by Gauss-elimination of $\mathbf{K}^{j+1/2}\mathbf{c}^{j+1} = \mathbf{D}^{j+1/2}\mathbf{c}^j$. $\mathbf{K}$ and $\mathbf{D}$ are matrices evaluated at the $j + 1/2$ level. The derivatives were discretized using central differences for the second derivative and either central differences or a third order quadratic upstream differencing scheme[28] for the first derivative $\partial c/\partial x$. The two differencing schemes for $\partial c/\partial x$ gave similar results under the velocity conditions of the simulations in the present study. At higher velocities used to test algorithm stability, third order upstream differencing prevented spurious oscillations (found with central differences) with minimal numerical diffusion. The coefficients, A_i, used to assemble $\mathbf{K}$ and $\mathbf{D}$ were formulated from Eqs. (2)–(4).

Determination of c^{j+1} gave significantly improved values for the free and bound concentrations at the $j + 1/2$ intermediate time level by a simple averaging procedure. To establish convergence criteria for all species required consideration of error terms. For a system with N species (either free or bound) in a domain with M grid points (e.g., 51 nodes for the 0.5-cm gel) there are $2NM$ error terms for each iteration. We calculated the error for each species as the difference in the concentration values between two iterations divided by the value of the concentration at the previous iteration. Finally, the total error was defined as the sum of the errors over the entire domain and over all the species concentrations (free and bound) for each iteration level. This method of iteration, which iterates toward global convergence, is superior to a "cascade" type scheme in

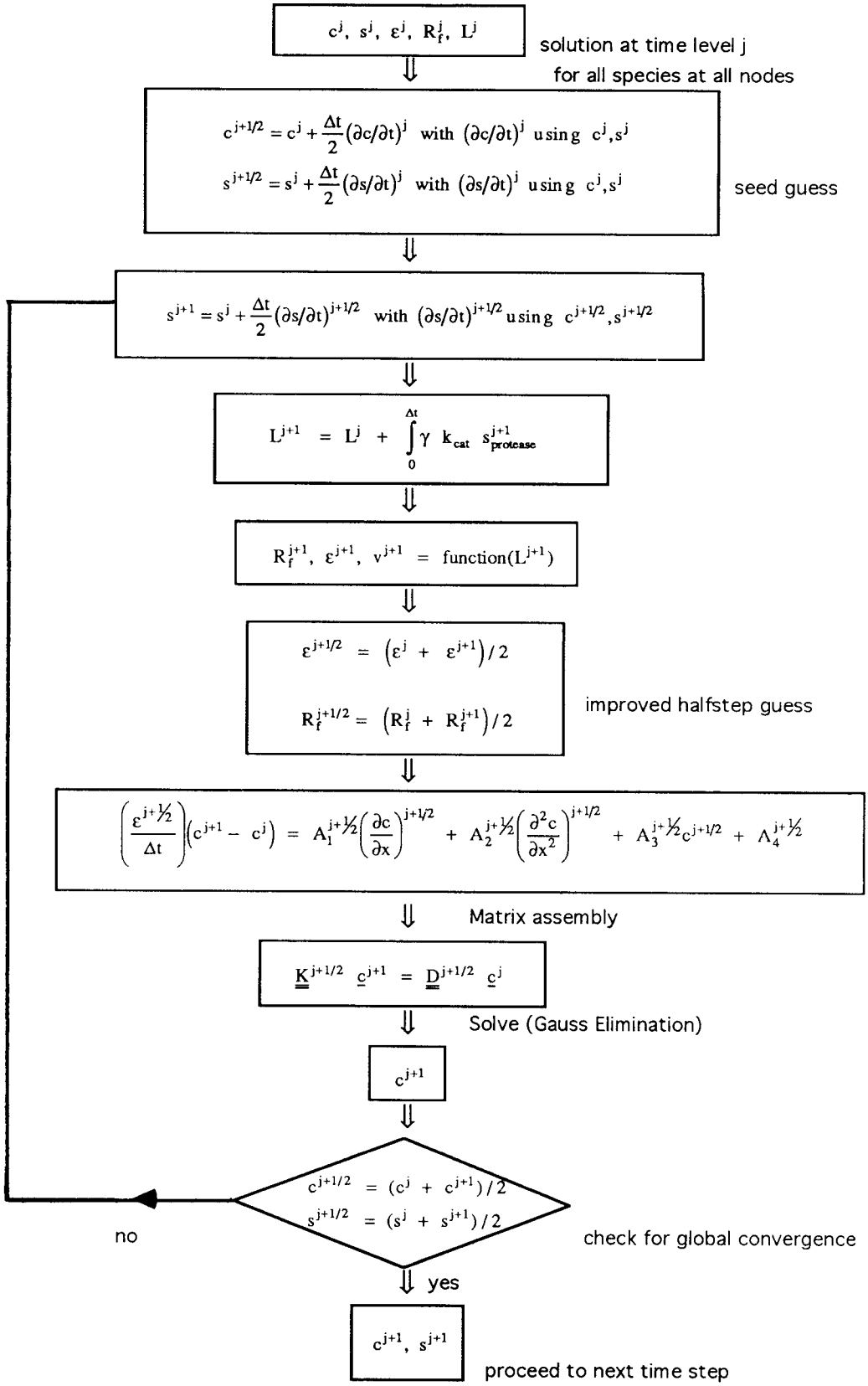

Figure 3. Iterative solution algorithm to solve the coupled system of PDEs for each species concentration in the fluid phase (c_i) or the solid phase (s_i) using a finite difference method.

which the iteration proceeds by sequentially seeking convergence of one species after another. Because species reactions are strongly coupled, such a scheme would be difficult to implement and inefficient. If the total error of the iteration was found to be less than a specified tolerance (typically 0.01) the iteration was stopped and the solution was advanced to the next time level. On the other hand, if the total error was larger than the tolerance then the iteration was continued with the newly obtained values at the $j + 1/2$ level as the seed guesses for the next iteration. We have observed a fairly rapid rate of convergence (requiring 1 to 25 iterations) which was monotonic and related to the magnitude of the time step (typically, $\Delta t = 0.01$ to 1 s). For simulations with 10 fast-reacting and convecting species through erodible media, a simulation of 30 min of lysis required under 4 h of CPU (Silicon Graphics R4000) time using $\Delta t = 0.01$ s and 0.01-cm node spacing.

With this method, the iteration approaches the correct solution without oscillation. The accuracy of the method can be augmented by using more terms in the Taylor series and weighting of the improved estimate before proceeding to the next iteration, but neither of these adjustments were needed. The principal criterion used to evaluate the solution obtained by our algorithm was the conservation of mass as reacting species that adsorb and desorb with an eroding phase. The conservation of mass of each species for the total system (both free and bound phases) has been rigidly implemented to within 0.5% for these simulations for over 10 species. Using analytical solutions to the diffusion and convection-diffusion, we have compared our solution with the analytical solutions in the special case where no reactions occur (porosity = 1.0) and have found agreement with the analytical solution with Peclet numbers from 0 to 500 (data not shown).

EXPERIMENTAL METHODS

Reagents

Purified human thrombin was obtained from Sigma Chemical Co. (St. Louis, MO) as a lyophilized powder (specific activity 3000 NIH U/mg). Lyophilized human fibrinogen (grade L, Kabi AB) was dissolved in 0.05 *M* Tris-HCl (pH 7.4), dialyzed, centrifuged, and the supernatant was frozen in small aliquots at −75°C. Purified human glu- and lys-plasminogen and human plasmin (American Diagnostica Inc., Greenwich, CT) were reconstituted, centrifuged, and stored at −75°C. Recombinant human tPA was obtained as a gift from Dr. W. Bennett (Genentech, Inc., S. San Francisco, CA). Recombinant urokinase was obtained as a gift from Dr. A. Sasahara (Abbott Laboratories, Chicago, IL).

Polymerization of Fibrin Gels and Fibrinolysis Experiments

Fibrin gel lysis experiments were carried out at 37°C in an environmental room.[61] Purified fibrin gels (2 cm long) were formed by prompt suction pipetting within 15 s of a rapidly mixed solution of fibrinogen (3 mg/mL) and thrombin (1 U/mL) into 100-μL glass capillary tubes (1.5 mm i.d.). The buffer for fibrin polymerization was 0.05 *M* Tris-HCl, 5 m*M* $CaCl_2$ (pH 7.4) with 0.1 *M* NaCl to obtain turbid, coarse gels.[7] Contrast-enhanced DIC microscopy of these gels has demonstrated that they are highly isotropic[61] with no fiber alignment due to flow prior to polymerization. In some experiments, glu-plasminogen (2.2 μ*M*) was copolymerized with the fibrinogen. To achieve lysis under conditions of permeation, purified fibrin clots were lysed with a 50-μL addition of lytic enzyme that was carefully loaded above the clot. The tube containing the fibrin clot was connected using tubing filled with 0.05 *M* Tris-HCl buffer to achieve a hydrostatic pressure head across the clot from 1 to 20 cm H_2O.[6,61] Degradation of the clot was monitored within 5 min of addition of plasmin, urokinase, or tPA. Volumetric flowrate was measured throughout the experiment. In diffusion-controlled lysis experiments (i.e., at zero pressure drop), clots were lysed by loading 50 μL of enzyme solution adjacent to the clot. The capillary was sealed at both ends to eliminate any macroscopic convective flow and held horizontally during the experiment. Changes in the position of fluid–gel interface were recorded with time as the clot lysed. For microscopic observation of lysis fronts, a double coverslip chamber provided for a parallel plate geometry for the creation of fibrin gels. A Leitz Aristoplan DIC microscope with 1.32 nA-planapo 100× oil immersion objective lens and 1.4-nA oil immersion condenser allowed real-time visualization of fibrin fibers. Dynamic experiments were recorded with a CCD72 (Dage-MTI) video camera with real-time digital contrast enhancement and background subtraction using an Argus 10 image processor (Hamamatsu Corp.).

RESULTS

Simulations and Measurement of Fibrinolysis Under Conditions of Diffusion

Placement of lytic solutions adjacent to fibrin gels caused sharp lysis fronts to move across the gels that were visible at all times of the experiments. Sharp fronts proceeded under conditions of diffusion for several hours when human glu_1-plasmin or lys_{77}-plasmin were placed adjacent to coarse fibrin or when uPA or tPA were placed adjacent to coarse fibrin copolymerized with glu-plasminogen. This was consistent with computer simulations of fibrinolysis in which very sharp lysis fronts occurring over 0.05-mm domains were predicted. For comparison with experimental data, the position of the lysis front was defined as the leading position at which 50% lysis was achieved. In the simulations without convection, the position of the fibrinolysis front was proportional to $t^{1/2}$, as expected for moving front processes controlled by the rate of diffusion.[10] At low enzyme concentrations of lys_{77}-plasmin, uPA, or tPA less

than 1 μM, the experimentally measured lysis front position also propagated in a manner nearly proportional to $t^{1/2}$. However, at high enzyme concentrations (plasmin = 10 μM; uPA or tPA > 1 μM), the front positions were correlated with $t^{1.0}$ and moved at nearly constant velocity and at speeds faster than simulated for diffusion-mediated transport, indicating non-Fickian behavior.

In fibrinolysis experiments under diffusion conditions, the placement of lys_{77}-plasmin adjacent to a coarse fibrin gel (3 mg fibrin/mL) resulted in a well-defined lysis front that moved at a rate dependent on the plasmin concentration (Fig. 4A). The cleaved form of plasmin was used to avoid the need to simulate the autocatalytic conversion of glu_1-plasmin to lys_{77}-plasmin. In Figure 4A, the computer simulation accurately predicted the front position using the kinetic constants of Table II for plasmin concentrations less than or equal to 1 μM. In the simulations, fibrin-bound plasmin has been assumed be released as a free species during fibrin solubilization. The rate constant of k_{cat} = 5 s^{-1} for the average bond cleavage rate by bound plasmin provided the best simulation of the data at 0.01, 0.1, and 1.0 μM plasmin. This value was consistent with independent measurements of fibrinogenolysis ($\gamma \cdot k_{cat}$ = 0.479 for fragment X generation[62]) and other estimates of the cleavage rate.[34,52] Also, this value of k_{cat} = 5 s^{-1} for plasmin-mediated cleavage of fibrin allowed accurate simulation of uPA- and tPA-mediated lysis fronts moving across plasminogen-laden fibrin (Fig. 4B and C) when the plasminogen activator levels were below 1.0 μM. Plasminogen activator kinetic parameters were from Table II for recombinant human tPA and two-chain uPA. In the simulations, 2.2 μM glu-plasminogen was in equilibrium with the fibrin as an initial condition. As was seen with plasmin, the simulations significantly underpredicted front movement at higher enzyme levels.

We have repeatedly observed unusually fast reaction front movement (front velocity > 0.1 mm/min) sustained for 2 h under conditions of high enzyme concentrations in over 30 independent measurements with various reaction cocktails.[61] For a reaction front to move 10 to 20 mm in 150 min by protein diffusion is anomalous. In the simulations of plasmin-mediated lysis, a diffusion coefficient that was five times greater than the real value was needed to estimate the rapidity of this front movement (Fig. 4A). Setting k_{cat} to an unrealistic level of 1000 s^{-1} (to illustrate the diffusion limited movement of the predicted lysis front) also substantially underpredicted the actual position and speed of the lysis front when 10 μM plasmin was placed adjacent to fibrin.

In light of the strong evidence for non-Fickian and anomalous transport in our experiments when compared with simulations of the process, we investigated the source of transport facilitation that caused the front to move faster than diffusion would dictate. Using contrast-enhanced DIC microscopy, we have demonstrated that fibrin fibers retracted under conditions of lysis in a region only 1 to 3 μm away from the lysis front as shown in Figure 5. The mo-

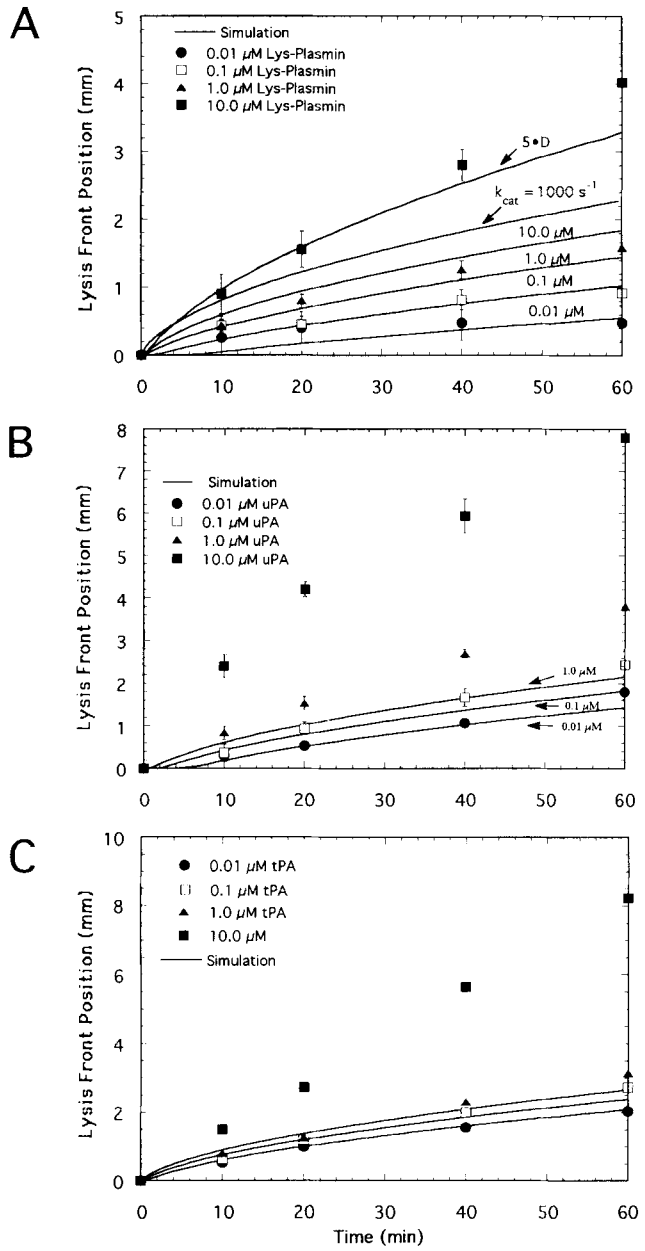

Figure 4. Comparison of model predictions (solid lines) with experimental measurements of lysis front movement across non-crosslinked fibrin gels under conditions of diffusion-mediated transport. The value of k_{cat} was set to 5 s^{-1} for the rate of fibrin cleavage by plasmin. The distance moved by the lysis front is plotted against time for four different doses of plasmin placed adjacent to the fibrin (A). The comparison revealed good agreement between observed and predicted front position for physiological (<2.2 μM) concentrations of plasmin placed adjacent to the fibrin gel. At 10 μM plasmin, the simulation significantly underpredicted lysis front movement, even at diffusion-limited conditions (k_{cat} = 1000 s^{-1}) as shown. This rapid front movement at 10 μM plasmin required an effective diffusion coefficient five times greater than the real value (5 · D_o). Comparison of predicted and observed lysis front positions is presented for lysis mediated by different dosages of uPA (B) or tPA (C) placed adjacent to the fibrin gel. Simulations (solid line) were run at enzyme concentration of nearest data as indicated. Each data point is the average of at least three independent determinations.

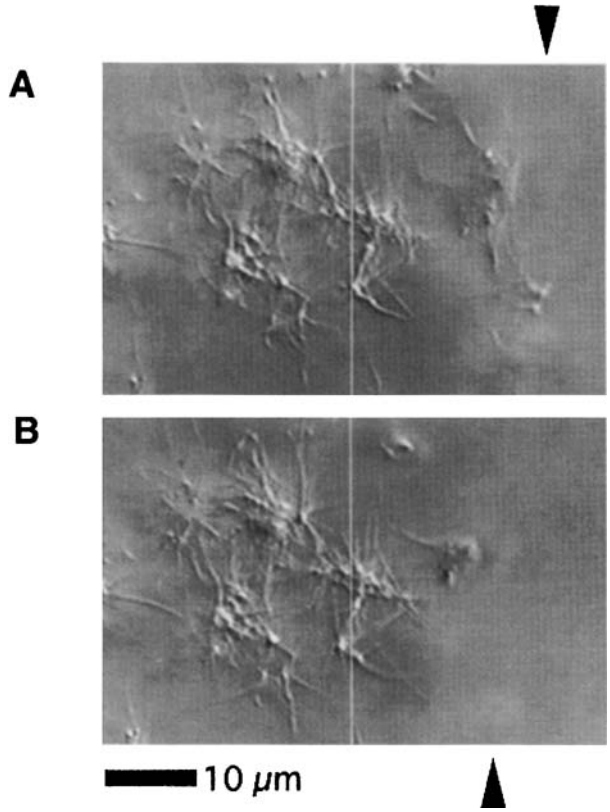

Figure 5. Experimental demonstration of protease-mediated fibrin fiber retraction at the lysis front. Plasmin at 1 μM was placed adjacent to fibrin (3 mg/mL). Fibers that are more than 5 μm away from the lysis front remain stationary, while within microns of the reaction front, the fibers retracted away from the front, thus convecting enzyme-laden fibers at a rate faster than diffusion. The top panel shows the position of the lysis front at a reference time while the bottom panel shows the lysis front 40 s later. The white line is used as a stationary marker to show a large scale movement of fibers across the line as the front nears that indicated position. The front is moving from right to left.

lecular origin of this retraction is not known but also occurred when 10% SDS was placed adjacent to fibrin gels. During proteolysis, protein degradation, denaturation, or loss of conformation may cause: (i) increased hydrophobic interactions; (ii) protein aggregation; and/or (iii) release of molecular tension within the degrading fibrin fiber. It is known that the fibrin monomer is stretched upon incorporation within the protofibril to maintain register. Alternatively, relaxation of stress gradients in fibers at the fluid/gel boundary related to the osmotic pressure gradients[47] across the boundary may occur under nonequilibrium conditions, and may drive the retraction near the lysis front. Also, relaxation of osmotic stress gradients at the outer radius of the dissolving fiber may contribute to fiber retraction during lysis. Regardless of its molecular origin, the retraction of fibers due to proteolysis was an observable front-sharpening mechanism (that confined lysis to a very narrow zone for long times) and facilitated transport of the proteins bound to fibers at rates that exceeded those predicted for classical diffusion.

With respect to other transport facilitation mechanisms, the following aspects require consideration. The rapid front movement was seen under isothermal conditions in an environmental room (±0.1°C), thus temperature fluctuations were not likely involved. Soret effects from heat generation due to bond cleavage are likely infinitesimal given the high thermal conductivity of water to dissipate thermal gradients. Because no bulk solvent flow into the gel was possible under the conditions of the experiments, osmotic effects were not responsible for the transport facilitation because osmotic pressure would not be expected to selectively move a solute. Additionally, the placement of blue dextran (10,000 MW) adjacent to fibrin gels or pure buffer showed that uncontrolled convection in the 1.5-mm-diameter capillary was minimal within the time frame of the experiment. During proteolysis, each peptide bond broken will release a proton. However, the experiments were conducted under buffering conditions that resulted in pH changes of less than 0.1 pH unit within 1 mm of the lysis front as measured with a small pH probe. Acidification of a negatively charged polymer like fibrin could result in shrinkage by reduction of strand repulsion. Yet, placement of a buffer solution at pH 5.0 adjacent to fibrin gels caused no change in the fluid/fibrin boundary. This suggested that the gel was not shrinking at the lysis front due to electrostatic effects during lysis.

Simulation and Measurement of Fibrinolysis Under Perfusion Conditions

Experiments were carried out by placing different concentrations of plasmin or uPA adjacent to a fibrin gel and imposing a constant hydrostatic pressure head across the gel causing convective delivery of the enzyme into the fibrin via permeation. Increasing the pressure drop across the gel enhanced the rate of lysis of fibrin by, typically, 10- to 25-fold compared with diffusion-mediated transport.[11,61] From these constant pressure drop experiments, the quasi-steady-state lysis front velocity was correlated with the quasi-steady-state superficial velocity, both of which remained essentially constant for at least 15 min during runs that lasted up to several hours (Fig. 6A and B). For the simulations, no estimate of the permeability was needed because the superficial velocity was available. The motivation of this comparison was to verify whether the value of $k_{cat} = 5\ s^{-1}$ for plasmin-mediated fibrinolysis, determined from the diffusion experiments, was suitable to simulate lysis front movement under conditions of convective transport. In Figure 6A, we present the comparison between experiment and simulations for lysis using 1.0 μM plasmin permeating into 3 mg/mL fibrin at various superficial velocities. In Figure 6B, a similar comparison is given for permeation of 1.0 μM of uPA into fibrin at various superficial velocities.

We observed good agreement between simulations and experimental data, indicating the appropriateness of the model and the kinetic rate constants. For both the plasmin and uPA permeation experiments, the model predicted, within the experimental scatter of the data, an upper limit

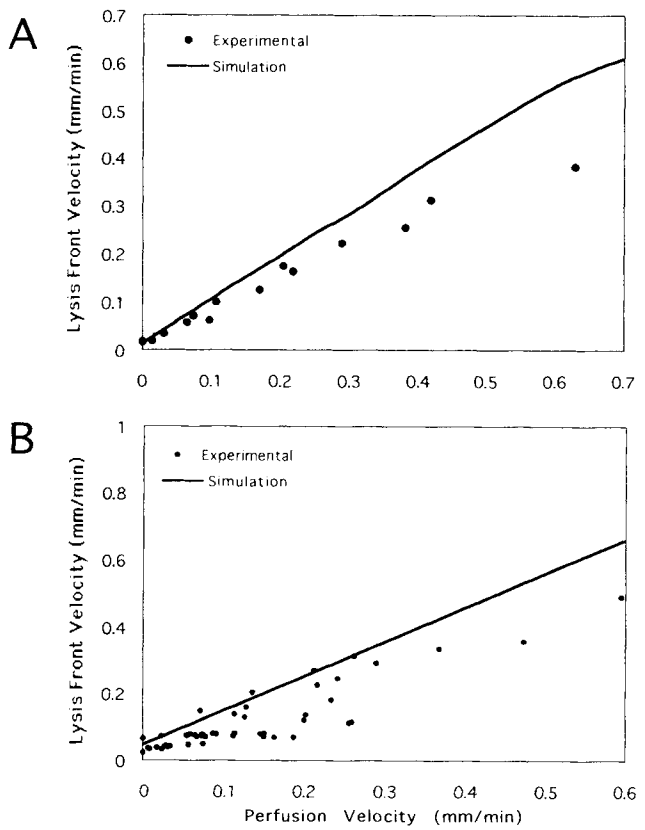

Figure 6. Comparison of model predictions (solid lines) with experimental measurements for lysis of non-crosslinked fibrin gels conducted under conditions of fluid permeation at constant pressure head. Fibrinogen (3.0 mg/mL) was polymerized with 1 U/mL thrombin in 0.1 *M* NaCl. (A) Plasmin (1 μM) was then placed on top of the coarse gel and introduced into the fibrin gel at varying initial pressure drops from 0 to 1.85 mmHg/cm (A). The perfusion velocity was measured during the course of lysis and the mean experimental velocity was used as input for the simulation. uPA (1 μ*M*) was placed on top of the gel (fibrin with 2.2 μ*M* plasminogen) and introduced into the gel at constant pressure drops of 0 to 1.85 mmHg/cm (B).

for the lysis front velocity at a given superficial permeation velocity. It is possible that there exists a contribution of the fiber retraction in our estimate of k_{cat} for plasmin-mediated fibrinolysis calculated from the diffusion experiments. This contribution would cause an overestimation of k_{cat} and the lysis front velocity. In addition, in the uPA permeation experiment, glu-plasminogen was copolymerized in the fibrin. At this point, we have not modeled glu_1-plasminogen conversion to lys_{77}-plasminogen or glu_1-plasmin conversion to lys-plasmin by glu_1- or lys_{77}-plasmin. Also, we have not delineated between the rates of glu-and lys-plasmin-mediated fibrinolysis.

Simulation of Published Data

Validation of the model presented in this article was attempted by comparing the predicted values of clot lysis times to those observed by Rijken et al.[42] For this comparison, we employed the value of $k_{cat} = 5.0\ s^{-1}$ for plasmin-mediated fibrinolysis, which had been used to simulate the data for diffusion and permeation mediated lysis. In the simulations, the kinetic parameters for the activation of plasminogen by single-chain tPA (obtained from Bowes melanoma cells) were those published by Rijken et al.[42] Rijken et al. give the fibrin lysis times for increasing doses of tPA in a well-mixed fibrin system. The criterion for complete solubilization of the fibrin was not available and, hence, a value of 95% lysis was used to predict the solubilization time. The model predictions of the time to lyse the clot were in close agreement with the published data (Fig. 7), but were slightly faster than observed experimentally by Rijken. These simulations were very sensitive to the value of k_{cat} used for plasmin-mediated fibrinolysis, and the overprediction of lysis rates (and consequent under prediction of lysis times) may be due to a slight overestimate of k_{cat} as discussed in the preceding section. The generation of carboxyterminal lysine residues for enhanced binding in degraded fibrin with the onset of significant lysis[50,53] may account for the more rapid decrease in clot lysis times with increase in the amount of activator (note the steeper slope of the experimental data). This effect was not incorporated in the present model and may account for the slightly lower slope in our simulations.

Simulation of Fibrinolysis in a Well-Mixed System in the Presence of Inhibitors

The preceding sections have focused on overall lysis rates and lysis front movement, both of which are important to the goal of achieving rapid reperfusion during thrombolytic therapy. The model also can calculate the instantaneous

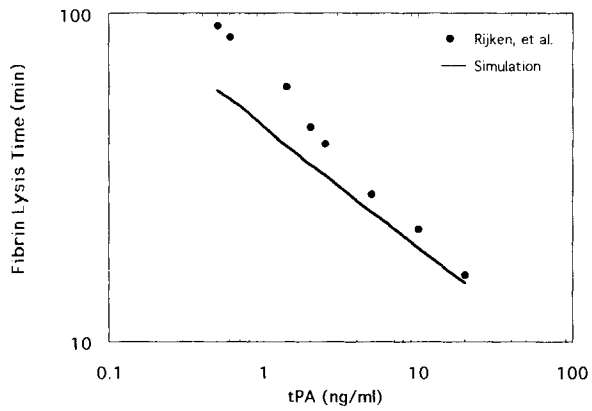

Figure 7. Comparison of model predictions with published data for lysis of purified fibrin by tPA-mediated activation of plasminogen.[42] The lysis time of clots formed in the presence of plasminogen is shown for different dosages of single-chain tPA. The initial concentration of fibrin was used to calculate the parameters to be used as input for the simulation. The fibrin concentration in these simulations was 5.88 μ*M*, the fibers were assumed to be coarse with a radius of 250 nm and the initial plasminogen concentration was taken to be 7.462 μ*M*. The kinetics for the activation of plasminogen by single-chain tPA were taken from Rijken et al.[42] as $k_2 = 0.22\ s^{-1}$ and $K_m = 2.42$ μ*M*. A value of $k_{cat} = 5\ s^{-1}$ was used for the rate of cleavage of fibrin by plasmin.

concentration of each species in the interstitial fluid and on the fibers of the dissolving fibrin.

We have run simulations for fibrinolysis mediated by tPA (Fig. 8A–C) or uPA (Fig. 8A′–C′) under well-mixed reaction conditions. At time equal to zero, either 50 nM of tPA or uPA was added to 3 mg/mL fibrin (250-nm-radius fibers) that contained 2.2 μM glu-plasminogen, 1.0 μM α_2-antiplasmin, and 0.01 μM PAI-1. The plasminogen was equilibrated with the fibrin prior to input of the plasminogen activator. The plasminogen initially bound to the fibrin was about 30% of the total plasminogen in the system. Initially, no plasmin or inhibited complexes were present. For tPA-mediated lysis, the bound plasminogen was rapidly converted to plasmin (Fig. 8A) by the adsorbing tPA. The concentration of PAI-1 dropped very rapidly by complexation with the tPA within 10 s (results not shown). At about 33 s, all the plasminogen initially bound to fibrin was converted to plasmin, and subsequent increases in the bound

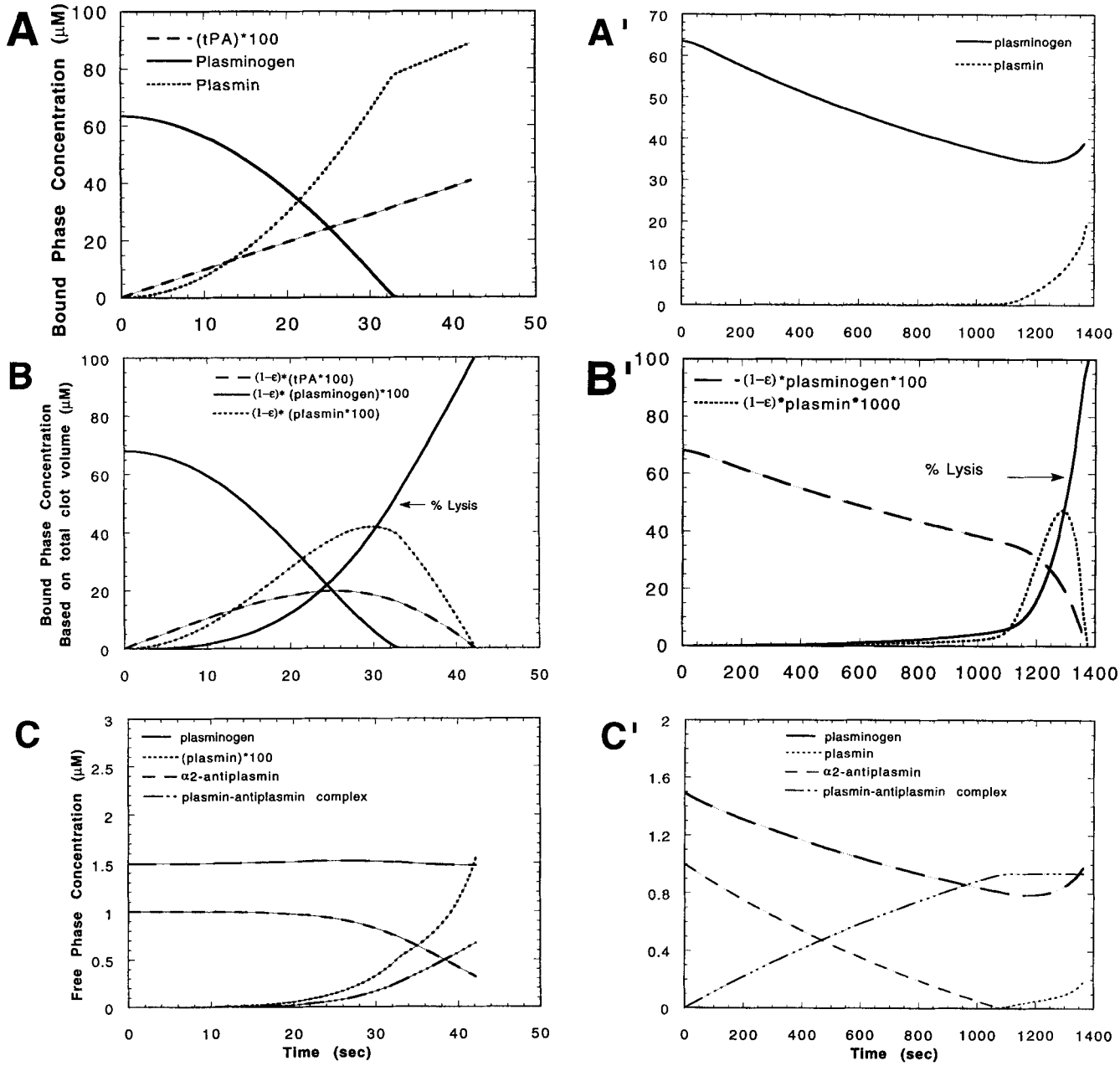

Figure 8. Fibrinolysis of a coarse plasma clot pre-equilibrated with 2.2 μM plasminogen. Simulation of lysis of a plasma clot (3 mg/mL, 8.823 μM) with coarse fibers (R_{fo} = 250 nm) was for a well mixed system with no spatial gradients in the problem. The plasminogen was activated by 50 nM tPA (A–C) or 50 nM uPA (A′–C′) in the presence of 1.0 μM α_2-antiplasmin and 10 nM PAI-1. The dynamic bound phase concentrations of plasminogen, plasmin, and tPA in the fibrin fibers are shown as a function of time (A, A′). The fluid phase concentrations of plasminogen, plasmin, α_2-antiplasmin, and the plasmin–antiplasmin complex are shown (B, B′). The dynamics of the bound phase concentration of plasminogen, plasmin, and tPA based on the total clot volume are shown (C, C′). The concentration of bound species based on total volume was obtained by multiplying the fibrin phase concentration by the ratio of the instantaneous solid volume to total volume, a factor equal to $1 - \epsilon(t)$. Also shown is the overall percent lysis as a function of time.

plasmin concentration were due to readsorption of free plasmin that had been solubilized and rapid conversion of adsorbing plasminogen by the high levels of tPA in the fibrin fibers. As lysis proceeded, the local concentration of species in the remaining volume of fibrin fibers increased; however, because the fiber volume was continually decreasing, the total amount of tPA or plasmin bound to fibrin in the two-phase system went through a maximum and then to zero as the fibrin was completely lysed (Fig. 8B). As lysis accelerated, the concentration of α_2-antiplasmin dropped as plasmin was released from the dissolving fibers and antiplasmin–plasmin complex formed in the free phase (Fig. 8C). The concentration of free plasmin remained below 20 n*M* at the end of the simulation and about 30% of the plasminogen in the system had been activated. During the simulation, the plasmin generated in the fibrin phase was protected from antiplasmin inhibition when bound to fibrin, but the plasmin solubilized into the free phase was immediately complexed with the antiplasmin. It is known[58] that plasmin on the fibrin phase is protected by free phase inhibition by α_2-antiplasmin and, hence, is free to degrade fibrin. In general, a 100% lysis time under 1 min for the dissolution of clotted plasma using 50 n*M* tPA (uniformly distributed) is a very reasonable estimate of the real process.

For dissolution under identical initial conditions to those of Figure 8A–C, where 50 n*M* uPA was used instead of tPA, we have found a markedly different pattern of lysis (Fig. 8A′–C′). After uPA was added, the rapid activation of free phase plasminogen to plasmin was not productive, because the plasmin was rapidly complexed by antiplasmin. The complexation of uPA with PAI-1 was essentially complete within the first 10 s of the simulations (data not shown). For the first 1100 s of the simulation, very little lysis occurred (<10%) due to the quenching effect of the antiplasmin. In this well-mixed system, the depletion of free phase plasminogen caused some desorption of the initial bound plasminogen due to re-equilibration, with a consequent drop in the bound phase concentration. At 1100 s, when no antiplasmin was left, the concentration of the antiplasmin–plasmin complex was not equal to the initial antiplasmin concentration because there was a small dilution effect due to loss of solid phase volume and gain of free phase volume as well as a small amount of antiplasmin in the plasminogen–antiplasmin complex. After 1100 s, plasmin began to accumulate in the free phase due to uPA-mediated activation. This plasmin rapidly bound fibrin and produced a dramatic burst of lysis. During this robust period of lysis, bound plasminogen was released into the free phase that could re-equilibrate with diminishing quantities of fibrin. The amount of plasminogen and plasmin bound to fibrin in the total two-phase system went to zero as the fibrin phase was completely dissolved.

In a simulation using 25 n*M* each of tPA and uPA added to fibrin at initial conditions used in Figure 8, the tPA in the system allowed for rapid generation of fibrin bound plasmin which was not susceptible to inhibition by antiplasmin. The fibrin lysed within 1 min as was seen in Figure 8A–C. There was little contribution by the urokinase in the system, except to compete for PAI-1 and maintain moderately higher levels of tPA in the free phase.

Simulation of Thrombolytic Therapy of Compacted Clot at Arterial Pressures

Arterial thrombi are formed dynamically under flow conditions. Platelet retraction can reduce plasma volume to 10% of its original volume and squeeze out much of the free phase plasma that is rich in plasminogen.[43] The large hydrodynamic forces of the arterial system may further compact the fibrin to about 5% of its original volume. Platelets release active PAI-1 into the clot which is a labile protein with a half-life of about 20 min. We have assumed that 30% of the plasma level of antiplasmin is within the clot. Typical intravenous thrombolytic therapy with tPA involves a bolus injection followed by continuous infusion. The plasma level of PAI-1 is as low as 0.5 n*M* and the plasma level of plasminogen and antiplasmin is 2.2 μM and 1.0 μM, respectively. The pressure drop across a 1-cm-long clot was estimated to be that between the arterial and venous circulation, about 60 mmHg.

We have simulated arterial thrombolytic therapy for a 15-mg tPA bolus into the systemic circulation (well-mixed volume of 5.5 L) followed by a 50-mg tPA infusion over 30 min. Due to removal of circulating tPA by the liver, recombinant human tPA has a half-life of about 5 min. The inlet condition into the clot (at $x = 0$) for tPA with time is the analytical solution of a first order decay process in well-mixed systemic circulation with a source term. We have assumed that the platelets in the clot create an initial PAI-1 level that is 50 times higher than plasma levels. The pressure drop of 60 mmHg/cm clot gives rise to an initial superficial permeation velocity of 2.529×10^{-4} cm/s across the clot. This velocity is based on the specific permeability for fibrous media calculated at all positions by the Davies equation, where $k = (2R_f)^2/\{70(1 - \epsilon)^{3/2} \cdot [1 + 52(1 - \epsilon)^{3/2}]\}$ for coarse, compacted fibrin ($R_{fo} = 250$ nm and $C_{fbn} = 60$ mg/mL).[11] As lysis proceeded, the superficial velocity increased.

We present the free and bound concentrations of species and inhibited complexes along with the percent lysis profiles across the clot. Within the first 10 min, the intravenous bolus of tPA caused a zone of complete lysis that had penetrated 0.13 cm into the clot (Fig. 9A). At a time of 10 min, a zone of partial lysis between 0.13 and 0.18 cm into the clot was present. In this partial lysis zone, fibrin-bound plasminogen was rapidly depleted by the bound tPA generating very high levels of plasmin bound to the fibrin (Fig. 9B). Behind the lysis front from $x = 0$ to 0.13 cm, the bound concentrations of species in the fibers were the residual levels of species left in vanishingly thin fibers—these concentrations reached high (millimolar range), but finite levels. These residual bound concentrations behind the front are in a zone of greater than 99.99% lysis and represent vanishingly small amounts of species. With respect to both

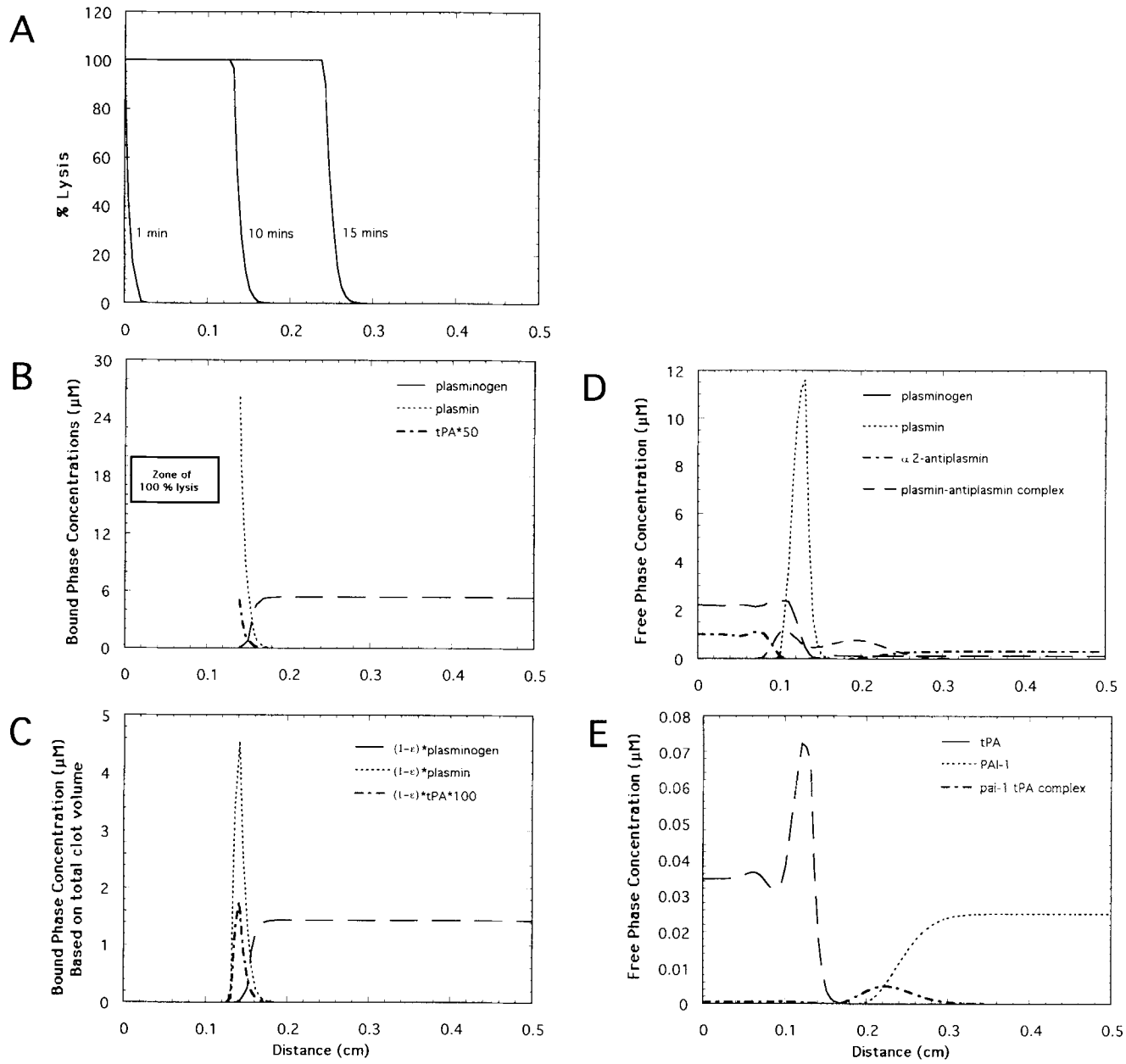

Figure 9. Fibrinolysis of an arterial thrombi mediated by tPA under conditions of arterial thrombolytic therapy. Simulations were for lysis of a flow-compacted clot (220 μM) generated from 3 mg/mL fibrin that had been equilibrated with 2.2 μM plasminogen. Thus the free plasminogen content was depleted to only 10% of its original value.[4,3] The permeation was driven by a pressure drop of 50 mmHg/cm clot leading to a superficial permeation velocity of 2.529×10^{-4} cm/s. At the inlet ($x = 0$), there was continuous infusion of 2.2 μM plasminogen, 1 μM α_2-antiplasmin, and 0.5 nM PAI-1. The initial clot concentrations were 0.3 μM α_2-antiplasmin and 0.025 nM PAI-1. A 15-mg bolus of tPA was followed by a continuous infusion of 50 mg of tPA for 30 min. The tPA has a half-life of 5 min in the systemic circulation (5.5 L). Spatial distribution of the percent lysis profiles are shown at 1, 10, and 15 min (A). The bound phase concentration profiles of plasminogen, plasmin, and tPA are shown at 10 min (B). The bound phase concentrations of plasminogen, plasmin, and tPA are shown based on the total clot volume at 10 min (C). The fluid concentrations of plasminogen, plasmin, α_2-antiplasmin, and the plasmin–antiplasmin complex are shown at 10 min (D) as well as the fluid phase concentrations of tPA, PAI-1, and the tPA–PAI-1 inhibitor complex at 10 min (E).

phases, no significant amount of plasmin(ogen) or tPA was actually bound to fibrin behind the front, as shown in Figure 9C. In fact, the zone that contained the peak amounts of plasmin and tPA bound to fibrin was at the active lysis front because both of these species adsorb to fibrin with high affinity. In this zone of partial lysis (which was advancing forward with time), the antiplasmin and PAI-1 in the free phase were completely depleted due to complexation events during the preceding 10 min (Fig. 9D and E). Because active uncomplexed tPA and plasmin can survive in the partial lysis zone, these two species were rapidly adsorbed by the dense fibrin structure as they permeated forward and then were subsequently solubilized. This led to a dramatic concentrating and continual accumulation of tPA and plas-

min in the zone of partial lysis which was moving forward across the clot. At 10 min, the concentration of the plasmin peak (x = 0.14 cm) exceeded initial plasminogen concentrations and was essentially equal to all the initially bound plasminogen from x = 0 to 0.14 that had been activated during the first 10 min minus the amount of plasmin in an inhibited complex. The fluid permeation front was actually ahead of this partial lysis zone, and this was seen with species that do not bind the fibrin such as with antiplasmin–plasmin complex and tPA–PAI-1 complex generated at earlier times in the simulation. Behind the lysis front, interesting reaction phenomena were also occurring in the fluid phase. Although all species are convecting forward, the sharp peak of plasmin in the free phase that existed in a zone of depleted antiplasmin was just ahead of a zone that was rich in free antiplasmin. Diffusion of plasmin from the peak toward the inlet into the antiplasmin-rich fluid resulted in rapid complex formation and a peak of complex that was lagging behind the main plasmin peak in the free phase (Fig. 9D and E). In the simulations, complexation between plasminogen and α_2-antiplasmin resulted in plasminogen–antiplasmin complex throughout the domain but the complex was at very nanomolar levels (data not shown).

Clinically, successful thrombolytic therapy with tPA provides for arterial reperfusion in 30 to 90 min. The simulations of this therapy, for a thrombus as defined above, indicated that substantial lysis can occur in the first 20 min. For clots that are several millimeters in length, the simulations provide quite reasonable prediction of actual reperfusion times.

Simulations of Collagenolysis

Up to this point, lysis of fibrin has been discussed. However, the numerical model is completely general and can accommodate structural and enzyme parameters for other fibrous systems such as collagen. In Figure 10 we present the results of our simulations using collagen based on parameters from Tables I and III. Collagenolysis is a very slow process[55] compared with fibrinolysis. Because only a limited number of outer fibrils participate in the binding of collagenase due to steric hindrance, we allowed only three shells of the fibrils [Eq. (17)] to be available for binding. As expected, the collagenase penetrated deeper into the collagen when the number of fibers available for binding was limited, thus reducing binding sites for adsorption. We observed that the rate of collagenolysis was significantly enhanced if all the collagen monomers in the fibers were sterically accessible; however, collagenase penetration was very poor due to strong binding. In effect, collagenolysis was enhanced in upstream regions of the gel and attenuated in downstream regions when all the fibrils participated in binding.

DISCUSSION

A two-phase, multicomponent model of enzymatic proteolysis predicted the dynamic and spatial patterns of dissolution of fibrous biopolymers. Considerable debate still exists on the ideal properties of a next generation thrombolytic agent. Also, administration regimes for plasminogen activators are continually being tested at great expense. The numerical model presented in this study will allow numerical optimization of different delivery schemes or enzyme parameters using one or more plasminogen activators. The reaction dynamics at the dissolution front have never been previously calculated, and we predict a particularly dramatic concentrating of active plasmin and tPA at the reaction front during the dissolution of arterial thrombi. These localized high levels of enzymes may be very relevant to the design of administration regimes where emerging evidence indicates a potential negative role for unusually high levels of tPA at the clot surface.[49,63]

The present model will be useful for optimizing thrombolytic administration regimes based on the biochemical properties of a given agent and a given type of thrombi. Calculation of systemic circulation dynamics can provide inlet conditions for the clot-dissolving simulation. The quantitative linkage between dosing and outcome (dissolution rate) can then be optimized for numerous regimens involving boluses and continuous intravenous infusions of uPA and tPA, with or without plasminogen supplementation. These optimizations would also seek to define therapeutic approaches in which enzymes were used most effectively, given existing transport constraints.

At present, the major species and reactions involved in the human fibrinolytic system have been incorporated in the numerical model. Comparison of the model with experimental systems using purified blood proteins has demonstrated that the human fibrinolytic system can be simulated accurately for conditions of diffusion at modest

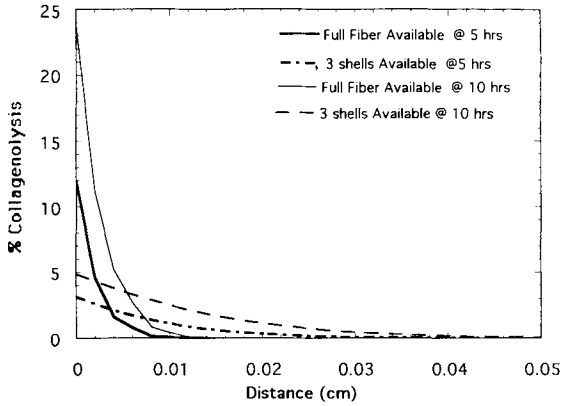

Figure 10. Collagen degradation under conditions of permeation. Spatial distribution of collagenolysis is shown after 1 and 5 h. Simulations are for a collagen gel of typical concentration (333 μM) with coarse fibers having an initial radius of 500 nm. The pressure drop was taken to be 50 mmHg/cm gel. The specific permeability was set at 10^{-13} cm^2 (see ref. 30) and the perfusion velocity was 6.67×10^{-7} cm/s. A concentration of 1 μM of human fibroblast collagenase was perfused into the gel at the constant pressure drop. The kinetics for the cleavage of collagen were assumed to be that for type I collagen (Table III). In one set of simulations, the whole fiber was available for binding of collagenase, whereas in the other set only three shells of the fibrils in the fiber were made available for binding.

enzyme concentrations (Fig. 4), permeation (Fig. 6), or in a well-mixed system (Fig. 7). Under conditions of robust lysis, a retraction occurs in dissolving fibrin fibers that facilitates enzyme transport in excess of rates predicted by diffusion alone. There has been no inclusion of a solid phase velocity (induced by proteolysis or by permeation-mediated compaction) in the transport equations.

Enzymes bound to an insoluble substrate can be solubilized back into solution as the substrate is dissolved. This mechanism for return of the enzyme to solution is important in eroding systems. As the mass of insoluble substrate decreases due to proteolysis, re-equilibration processes may drive the enzyme back into solution since there are fewer binding sites available. However, under conditions of rapid proteolysis, reversible adsorption need not be at equilibrium. To maintain conservation of mass under these conditions requires solubilization (a kinetic mechanism) to return enzyme to solution. To account for solubilization in our system, we combined a shrinking core and progressive conversion model by assuming the fiber is solubilized at constant density. Thus, reaction is uniform within the fiber, but we propose that mechanisms are present which cause contraction of the dissolving fibers to maintain constant density. In fibrin, this approach is supported by the longitudinal (this report) and radial[61] fiber retraction observed in dissolving fibers by digitally enhanced DIC microscopy. The high porosity of fibrin fibers ($\epsilon_{\text{fiber}} = 0.8$) and their small diameter (<1 μm) argue that adsorbing proteins may be relatively uniform throughout the fiber by bulk and surface diffusion mechanisms. For tPA which binds fibrin strongly, lysis may be more like a shrinking core phenomena. For uPA-mediated lysis, progressive conversion may be more suitable. Given the complexity of the system, our assumption of solubilization at constant fibrin density provided suitable approximation of the real processes for either activator. Little is known about the structural dynamics of collagen degradation. In the collagen model, it was possible to reduce the amount of monomer available for binding within the fiber due to steric hindrance. In eroding fibrous media, an important advantage in allowing fibers to shrink radially at constant density is the linkage of local reaction phenomena with transport properties that are dependent on local structure. Also, calculation of inner fiber concentration gradients was avoided with at least a 100-fold savings in computation time.

In comparison to our earlier modeling efforts,[11] we have added the inhibition reactions and incorporated the mechanism for solubilization of enzymes back into solution. In our previous work, return of enzyme to solution occurred by re-equilibration mechanism which was valid in the slow fibrinolysis regime. Also, we have treated plasmin-mediated fibrinolysis as a first order reaction instead of a Michaelis–Menten reaction. Because the cleavage site concentration near a bound plasmin molecule is so much higher than the apparent K_m, the Michaelis–Menten formulation reduces to a first order reaction in bound plasmin. The inclusion of antiplasmin in the reaction network required a very small time step because the complexation reaction of antiplasmin with plasmin is extremely fast. To capture more accurately the sharp fronts in the system, we have used greater node resolution ($\Delta x = 0.01$ cm) than in the previous study.[11] In future work, adaptive meshing may provide even more accurate simulation of the dynamics at the sharp reaction front. Also, in future work, we seek to study lysis phenomena in two-dimensional systems. The nonisotropic nature of real blood clots, with platelet-rich and platelet-poor regions may lead to preferred channels (dissolution fingering) of permeation and lysis. Retracted platelet-rich regions of the clot which are resistant to flow can direct fluids through more permeable regions of the clot. Such spatial variations in permeability can be described in a two-dimensional model, based on Eq. (1) where the permeability varies with position.

Proteolytic processes are commonly encountered in numerous biological matrices. With increasing knowledge of transport, adsorption, and reaction phenomena, the regulation or optimization of these processes for bioengineering or biomedical goals may be facilitated by use of computer simulation. This study has focused primarily on reactions in fibrin. Other complex biological systems are likely suited for investigation using the formulation presented in this study.

This work was supported by a National American Heart Association grant (No. 938670) and National Science Foundation grant (No. BCS 9358236) through the National Young Investigator Program. The authors thank Drs. J. Nitsche and C. Lund for helpful discussions.

NOMENCLATURE

c_i	free phase concentration of ith species based on fluid phase volume (μM)
D_i	diameter of ith species (nm)
$\mathcal{D}_i$	Brownian diffusion coefficient of ith species in water (cm/s^2)
$\mathcal{D}_{i,\text{eff}}$	effective diffusion coefficient of ith species in fibrous media (cm/s^2)
D_L	longitudinal dispersion coefficient (cm/s^2)
D_{pore}	pore diameter (nm)
k	specific permeability (cm^2)
k''	second order association rate (μM^{-1} s^{-1})
$k^r_{f,i}$	forward rate coefficient of ith species associating with rth site in solid phase (μM^{-1} s^{-1})
$k^r_{r,i}$	reverse rate coefficient of ith species dissociating from rth site in solid phase (s^{-1})
K_m	Michaelis constant (μM)
k_2	Michaelis–Menten kinetic rate constant (s^{-1})
k_{cat}	kinetic rate constant (s^{-1}) for solid phase bound protease
L	historic amount of cleavage (μM) based on solid phase volume
L_T	total length of fiber in gel
N_{av}	Avogadro's number
$m(R_f)$	total number of protofibrils present in a fiber of radius, R_f
MW	molecular weight
q_i	number of binding sites per monomer
R^i_{jk}	generation of ith species in fluid phase by interaction of j and k species (μM/s)
$^sR^i_{jk}$	generation of ith species in solid phase by interaction of j and k species (μM/s)
R_f	fiber radius (nm)

R_{fo} initial fiber radius (nm)
$\mathcal{R}$ instantaneous rate of cutting (μM/s)
r_o protofibril or microfibril radius (nm)
p_o protofibril density (nm^{-2})
s_i solid phase concentration of ith species based on solid volume (μM)
t time (s)
vol_T total volume of the clot
$\mathbf{v}$ convective velocity (cm/s) within the pore (averaged over local pore volume)
v_x axial convective velocity (cm/s) within the pore (averaged over local pore volume)
$\bar{v}$ superficial velocity (cm/s) based on total volume
x axial position (cm)

ϵ porosity of bed
ϵ_{fiber} porosity of fiber
ξ_{rj} interaction parameter allowing binding of jth species to rth site
κ number of shells of the fiber available for binding
γ solubilization parameter (equivalent moles solubilized/moles of cleavages)
θ_i total ith binding site concentration based on solid phase volume (μM)
ρ density of bed (mg/cm^3)
ρ_{fiber} density of fiber (mg/cm^3)

References

1. Bear, J., Bachmat, Y. 1991. Introduction to modeling transport phenomena in porous media. Kluwer, Norwell, MA.
2. Blinc, A. G., Planinsic, G., Keber, D., Jarh, O., Lahajnar, G., Zidansek, A., Demsar, F. 1991. Dependence of blood clot lysis on the mode of transport of urokinase into the clot-A magnetic resonance imaging study in vitro. Thromb. Haem. **65**: 549–552.
3. Blomback, B., Carlsson, K., Hessel, B., Liljeborg, A., Procyk, R., Aslund, N. 1989. Native fibrin gel networks observed by 3D microscopy, permeation and turbidity. Biochim. Biophys. Acta **997**: 96–110.
4. Blum, J. J., Lawler, G., Reed, M., Shin, I. 1989. Effect of cytoskeletal geometry on intracellular diffusion. Biophys. J. **56**: 995–1005.
5. Brenner, H., Gaydos, J. 1977. The constrained Brownian movement of spherical particles in cylindrical pores of comparable radius: Models of the diffusive and convective transport of solute molecules in membranes and porous media. J. Coll. Interf. Sci. **58**: 312–355.
6. Carr, M. E., Shen, L. L., Hermans, J. 1977. Mass–length ratio of fibrin fibers from gel permeation and light scattering. Biopolymers **16**: 1–15.
7. Carr, M. E., Hermans, J. 1978. Size and density of fibrin fibers from turbidity. Macromolecules **11**: 46–50.
8. Castellino, F. J. 1981. Recent advances on the chemistry of the fibrinolytic system. Chem. Rev. **81**: 431–447.
9. Collen, D., Zamarron, C. Lijnen, H. R., Hoylaerts, M. 1986. Activation of plasminogen by pro-urokinase. J. Biol. Chem. **261**: 1259–1266.
10. Crank, J. 1975. The mathematics of diffusion. Oxford University Press, New York.
11. Diamond, S. L., Anand, S. 1993. Inner clot diffusion and permeation during fibrinolysis. Biophys. J. **65**: 2622–2643.
12. Doolittle, R. F. 1984. Fibrinogen and fibrin. Annu. Rev. Biochem. **53**: 195–229.
13. Dullien, F. A. 1979. Porous media: Fluid transport and pore structure. Academic Press, New York.
14. Enghild, J. J., Salvesen, G., Brew, K., Nagase, H. 1989. Interaction of human rheumatoid collgenase (matrix metalloproteinase 1) and stromelysin (matrix metalloproteinase 3) with human α2-macroglobulin and chicken ovostatin. J. Biol. Chem. **264**: 8779–8785.
15. Fanti, I., Glandt, E. 1990. Partitioning of spherical particles into fibrous matrices. J. Coll. Interf. Sci. **135**: 396–404.
16. Fietzek, P. P., Kuhn, K. 1976. The primary structure of collagen. Int. Rev. Connect. Tissue Res. **47**: 1–60.
17. Finlayson, B. A. 1992. Numerical methods for problems with moving fronts. Ravenna Park Publishing, Seattle, WA.
18. Froment, G. F., Bischoff, K. B. 1990. Chemical reactor analysis and design. Wiley, New York.
19. Gabriel, D. A., Muga, K., Boothroyd, E. M. 1992. The effect of fibrin structure on fibrinolysis. J. Biol. Chem. **267**: 24259–24263.
20. Gupta, S. P., Greenkorn, R. A. 1973. Dispersion during flow in porous media with bilinear adsorption. Water Resources Res. **9**: 1357–1368.
21. Harris, E. D., Jr., Welgus H. G., Krane, S. M. 1984. Regulation of the mammalian collagenases. Collag. Rel. Res. **4**: 493–512.
22. Hekman, C. M., Loskutoff, D. J. 1988. Kinetic analysis of the interactions between plasminogen activator inhibitor 1 and both urokinase and tissue plasminogen activator. Archives Biochem. Biophys. **262**: 199–210.
23. Hoylaerts, M., Rijken, D. C., Lijnen, H. R., Collen, D. 1982. Kinetics of the activation of plasminogen by human tissue plasminogen activator. J. Biol. Chem. **257**: 2912–2919.
24. Husain, S. S., Hasan, A. A. K., Budzynski, A. Z. 1989. Differences between binding of one-chain and two-chain tissue plasminogen activators to non-cross-linked and cross-linked fibrin clots. Blood **74**: 999–1006.
25. Johannessen, M., Nielsen, F., Petersen, L. C. 1989. Plasmin catalyzed cleavage of single chain tissue-type plasminogen activator in fibrin clots. Fibrinolysis **3**: 215–220.
26. Kaufman, E. N., Jain, R. K. 1990. Quantification of transport and binding parameters using fluorescence recovery after photobleaching. Biophys. J. **58**: 873–885.
27. Kyan, C. P., Wasan, D. T., Kinter, R. C. 1970. Flow of single-phase fluids through fibrous beds. Ind. Eng. Chem. Fund. **9**: 596–603.
28. Leonard, B. P. 1979. A stable and accurate convective modelling procedure based on quadratic upstream interpolation. Comp. Meth. Appl. Mech. Eng. **19**: 59–98.
29. Levenspiel, O. 1972. Chemical reaction engineering. Wiley, New York.
30. Levick, J. R. 1987. Flow through interstitium and other fibrous matrices. Q. J. Exper. Physiol. **72**: 409–438.
31. Lijnen, H. R., Collen, D. 1982. Interaction of plasminogen activators and inhibitors with plasminogen and fibrin. Sem. Thromb. Hemostas. **8**: 2–11.
32. Lijnen, H. R., Van Hoef, B., Collen, D. 1991. On the reversible interaction of plasminogen activator inhibitor-1 with tissue-type plasminogen activator and with urokinase-type plasminogen activator. J. Biol. Chem. **266**: 40141–4044.
33. Lijnen, H. R., Van Hoef, B., De Cock, F., Collen, D. 1989. The mechanism of plasminogen activation and fibrin dissolution by single chain urokinase type plasminogen activator in a plasma milieu in vitro. Blood **73**: 1864–1872.
34. Lottenberg, R., Christensen, U., Jackson, C. M., Coleman, P. L. 1981. Assay of coagulation proteases using peptide chromogenic and fluorogenic substrates. Meth. Enzymol. **80**: 341–361.
35. Lucas, M. A., Fretto, L. J., McKee, P. A. 1983. The binding of human plasminogen to fibrin and fibrinogen. J. Biol. Chem. **258**: 4249–4256.
36. Ogston, A. G. 1958. The spaces in a uniform random suspension of fibers. Trans. Faraday. Soc. **54**: 1754–1757.
37. Park, I. H., Johnson, C. S., Jones, M. R., Gabriel, D. A. 1988. Probes of fibrin gel porosity. Proc. Int. Fibrinogen Workshop **3**: 123–126.
38. Peppas, N. A., Hansen, P. J., Buri, P. A. 1984. A theory of molecular diffusion in the intestinal mucus. Int. J. Pharm. **20**: 107–119.
39. Phillips, R. J., Deen, W. M., Brady, J. F. 1989. Hindered transport

of sperical macro-molecules in fibrous membranes and gels. AIChE J. **35**: 1761–1769.
40. Phillips, R. J., Deen, W. M., Brady, J. F. 1990. Hindered transport in fibrous membranes and gels: effect of solute size and fiber configuration. J. Coll. Interf. Sci. **139**: 363–373.
41. Ranby, M., Brandstorm, A. 1988. pp. 211–224. In: C. Kluft (ed.), Tissue-type plasminogen activator (t-PA). CRC Press, Boca Raton, FL.
42. Rijken, D. C., Hoylaerts, M., Collen, D. 1982. Fibrinolytic properties of one-chain and two-chain human extrinsic (tissue-type) plasminogen activator. J. Biol. Chem. **257**: 2920–2925.
43. Sabovic, M., Lijnen, H. R., Keber, D., Collen, D. 1990. Correlation between progressive adsorption of plasminogen to blood clots and their sensitivity to lysis. Thromb. Haem. **64**: 450–454.
44. Sahimi, M., Hughes, B. D., Scriven, L. E., Davis, H. T. 1986. Dispersion in flow through porous media—one-phase flow. Chem. Engr. Sci. **41**: 2103–2122.
45. Saltzman, W. M., Radomsky, M. L., Whaley, K. J., Cone, R. A. 1994. Antibody diffusion in human cervical mucus. Biophys. J. **66**: 508–515.
46. Seltzer, J. L., Eisen, A. Z., Bauer, E. A., Morris, N. P., Glanville, R. W., Burgeson, R. E. 1989. Cleavage of type VII collagen by interstitial collagenase and type IV collagenase (gelatinase) derived from human skin. J. Biol. Chem. **264**: 3822–3826.
47. Silverberg, A. 1980. The role of matrix mechanical stress in swelling equilibrium and transport through networks. Macromolecules **13**: 742–748.
48. Smith, G. D. 1985. Numerical solution of partial differential equations: Finite difference methods. Oxford University Press, New York.
49. Sobel, B. E., Nachowiak, D. W., Fry, E. T., Bergmann, S. R., Torr, S. R. 1990. Paradoxical attenuation of fibrinolysis attributable to "plasminogen steal" and its implications for coronary thrombolysis. Cor. Artery Dis. **1**: 111–119.
50. Suenson, E., Lutzen, O., Thorsen, S. 1984. Initial plasmin-degradation of fibrin as the basis of a positive feed-back mechanism in fibrinolysis. Eur. J. Biochem. **140**: 513–522.
51. Thorsen, S., Mullertz, S., Suenson, E., Kok, P. 1984. Sequence of formation of molecular forms of plasminogen and plasmin-inhibitor complexes in plasma activated by urokinase or tissue-type plasminogen activator. Eur. J. Biochem. **223**: 179–187.
52. Tiefenbrunn, A. J., Graor, R. A., Robinson, A. K., Lucas, F. V., Hotchkiss, A., Sobel, B. E. 1986. Pharmocodynamics of tissue-type plasminogen activator characterized by computer-assisted simulation. Circulation **73**: 1291–1299.
53. Tran-Thang, C., Kruithof, K. O., Atkinson, J., Bachmann, F. 1986. High-affinity binding sites for human glu-plasminogen unveiled by limited plasmic degradation of human plasmin. Eur. J. Biochem. **160**: 509–604.
54. Weisel, J. W., Nagaswami, C. 1992. Computer modeling of fibrin polymerization kinetics correlated with electron microscope and turbidity observations: Clot structure and assembly are kinetically controlled. Biophys. J. **63**: 111–128.
55. Welgus, H. G., Jeffrey, J. J., Stricklin, G. P., Roswit, W. T., Eisen, A. Z. 1980. Characteristics of the action of human skin fibroblast collagenase on fibrillar collagen. J. Biol. Chem. **255**: 6806–6813.
56. Welgus, H. G., Stricklin, G. P. 1983. Human skin fibroblast collagenase inhibitor: Comparative studies in human connective tissues, serum and amniotic fluid. J. Biol. Chem. **258**: 12259–12264.
57. Whitaker, S. 1987. Mass transport, and reaction in catalyst pellets. Transport Por. Media **2**: 269–299.
58. Wiman, B., Collen, D. 1977. Purification and characterization of a human antiplasmin, the fast-acting plasmin inhibitor in plasma. Eur. J. Biochem. **78**: 19–26.
59. Wiman, B., Collen, D. 1978. On the kinetics of the reaction between human antiplasmin and plasmin. Eur. J. Biochem. **84**: 573–578.
60. Wiman, B., Lijnen, H. R., Collen, D. 1979. On the specific interaction between the lysine-binding sites in plasmin and complementary sites in α2-antiplasmin and in fibrinogen. Biochim. Biophys. Acta **579**: 142–154.
61. Wu, J. H., Siddiqui, K., Diamond, S. L. 1994. Transport phenomena and clot dissolving therapy: An experimental investigation of diffusion-controlled and permeation-enhanced fibrinolysis. Thromb. Haem. **72**: 105–112.
62. Wu, J. H., Diamond, S. L. 1995. A fluorescence quench and dequench assay of fibrinogen polymerization, fibrinogenolysis, and fibrinolysis. Anal. Biochem. **224**: 83–91.
63. Wu, J. H., Diamond, S. L. 1995. Tissue plasminogen activator (tPA) inhibits plasmin degradation of fibrin: A mechanism that slows tPA-mediated fibrinolysis but does not require α_2-antiplasmin or leakage of intrinsic plasminogen. J. Clin. Invest. **95**:2483–2490.
64. Zamarron, C., Lijnen, H. R., Collen, D. 1984. Kinetics of the activation of plasminogen by natural and recombinant tissue type plasminogen activator. J. Biol. Chem. **259**: 2080–2093.